Holocene relative shore-level changes and development of the Ģipka lagoon in the western Gulf of Riga

ALAR ROSENTAU (iD), IEVA GRUDZINSKA, EDYTA KALIŃSKA (iD), HELENA ALEXANDERSON, VALDIS BĒRZIŅŠ, AIJA CERIŅA, LAIMDOTA KALNIŅA, JĀNIS KARUŠS, KRISTAPS LAMSTERS, MERLE MURU (iD), MĀRIS NARTIŠS, LĪGA PAPARDE AND TIIT HANG (iD)

BOREAS

Rosentau, A., Grudzinska, I., Kalińska, E., Alexanderson, H., Bērziņš, V., Ceriņa, A., Kalniņa, L., Karušs, J., Lamsters, K., Muru, M., Nartišs, M., Paparde, L. & Hang, T.: Holocene relative shore-level changes and development of the Ģipka lagoon in the western Gulf of Riga. *Boreas*. https://doi.org/10.1111/bor.12628. ISSN 0300-9483.

Holocene relative shore-level changes and development of the Ģipka palaeolagoon in the western Gulf of Riga are reconstructed using multiproxy analyses by combining litho-, biostratigraphical and chronological data with remote sensing and geophysical data. The results show the development of the Ģipka basin from the Ancylus Lake/Initial Litorina Sea coastal zone (before *c.* 9.1 cal. ka BP) to coastal fen (*c.* 9.1 to 8.4 cal. ka BP) and gradual development of the Litorina Sea lagoon (*c.* 8.4 to 4.8 cal. ka BP) and its transition to a freshwater coastal lake (*c.* 4.8 to 4.6 cal. ka BP), fen (*c.* 4.6 to 4.2 cal. ka BP), and river floodplain (since *c.* 4.2 cal. ka BP). The highest shorelines of the Ancylus Lake and Litorina Sea were mapped at an elevation of 12–11 and 9 m a.s.l., respectively. A new relative shore level (RSL) curve for the western Gulf of Riga was constructed based on RSL data from the Ģipka area and from nearby Ruhnu Island studied earlier. The reconstruction shows that the beginning of the last marine transgression in the western Gulf of Riga started at *c.* 8.4 cal. ka BP, and concurred with the 1.9 m RSL rise event recorded from the North Sea basin. Diatom analysis results indicate the existence of the Ģipka lagoon between *c.* 7.7 and 4.8 cal. ka BP, with the highest salinity *c.* 6.1 cal. ka BP. During the existence of the brackish lagoon, settlement sites of the Neolithic hunter–gatherer groups existed on the shores of the lagoon in the period *c.* 6.0 to 5.0 cal. ka BP.

Alar Rosentau (alar.rosentau@ut.ee), Merle Muru and Tiit Hang, Institute of Ecology and Earth Sciences, University of Tartu, Ravila 14A, Tartu 50411, Estonia; Ieva Grudzinska, Institute of Biology, University of Latvia, Jelgavas iela 1, LV-1004 Rīga, Latvia and Department of Environmental Sciences, University of Basel, Klingelbergstrasse 27, 4056 Basel, Switzerland; Edyta Kalińska, Nicolaus Copernicus University, Faculty of Earth Sciences and Spatial Management, Lwowska 1, Toruń 87-100, Poland; Helena Alexanderson, Department of Geology, Lund University, Sölvegatan 12, SE-223 62 Lund, Sweden and UiT the Arctic University of Norway, Dramsvegen 1, N-9009 Tromsø, Norway; Valdis Bērziņš, Institute of Latvian History, University of Latvia, Kalpaka bulvāris 4, LV-1050 Rīga, Latvia; Aija Ceriņa, Laimdota Kalniņa, Jānis Karušs, Kristaps Lamsters, Māris Nartišs and Līga Paparde, Faculty of Geography and Earth Sciences, University of Latvia, 1 Jelgavas Street, LV-1004 Rīga, Latvia; received 22nd June 2021, accepted 21st June 2023.

An interplay between glacial–isostatic adjustment (GIA) and postglacial sea-level rise in the slowly uplifting coastal areas of the Baltic Sea in SW Sweden (Berglund *et al.* 2005; Yu *et al.* 2007; Hansson *et al.* 2018), NW Russia (Sandgren *et al.* 2004; Miettinen *et al.* 2007), SE Finland (Miettinen 2004) and Estonia (Rosentau *et al.* 2013; Nirgi *et al.* 2020) has led to complex relative shore level (RSL) changes with multiple transgression–regression cycles (Fig. 1A). Because the differences in land uplift rates were quite small, in some of these areas the Litorina Sea highest shorelines (*c.* 7.5 to 6.5 cal. ka BP) are today located at lower elevation (Nirgi *et al.* 2020) compared with the older Ancylus Lake shores (*c.* 10.2 cal. ka BP), whereas in other locations the situation is reversed (Hansson *et al.* 2018). These sensitive areas are very suitable for the study of Holocene RSL changes and isostatic uplift in order to calibrate global GIA models (Tushingham & Peltier 1992; Lambeck *et al.* 1998) and to detect the melting episodes of large ice sheets during the Early to Middle Holocene.

After the damming and drainage of the Ancylus Lake, the last marine inundation of the Baltic Sea Basin (BSB) started at *c.* 9.8 cal. ka BP (Bennike & Jensen 2013), initiated by the inflow of saline waters from the North Atlantic. This transgression during the Early Holocene most likely followed the opening of the present-day Great Belt and Fehmarn Belt region (Feldens & Schwarzer 2012). Rising sea-level resulted in flooding of the southern Kattegat area *c.* 9.3 cal. ka BP (Bendixen *et al.* 2017). However, the timing of the transition from fresh to brackish water that marks the onset of the Litorina Sea is not yet clearly determined and might have started in the northern Great Belt region *c.* 9.0 cal. ka BP and east of the Darss Sill after 8.5 cal. ka BP (Andrén *et al.* 2011). The cause of the saline water inflow into the BSB is believed to be related to episodic melting of the Laurentide and Antarctic ice sheets and the resulting rapid sea-level rise events (Andrén *et al.* 2011). In the Blekinge area (SW Sweden) the initial transgression (L1) of *c.* 2.5 m took place between 8.5 and 8.2 cal. ka BP (Berglund *et al.* 2005), while the main transgression was centred around 7.6 cal. ka BP (Berglund *et al.* 2005; Yu *et al.* 2007). The latter is detected as a major RSL rise event also in the Gulf of Riga and Gulf of Finland areas,
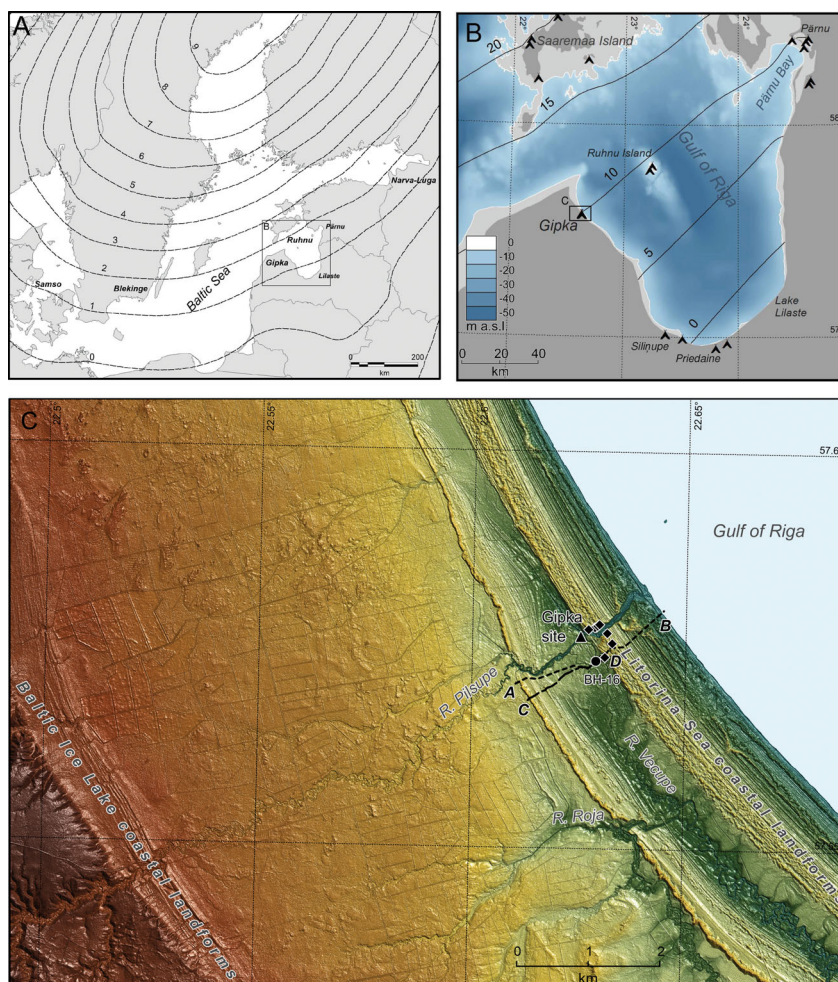
Fig. 1. A. Overview map of the Baltic Sea with the location of the study area, sites discussed in the text and present-day land uplift isobases (mm a⁻¹, Vestøl *et al.* 2019). B. Palaeogeographical reconstruction of the Litorina Sea maximum in the Gulf of Riga with relative shore-level (RSL) isobases at *c.* 7.3 cal. ka BP and with the most important Stone Age settlement sites around the gulf (after Muru *et al.* 2017). C. Airborne Lidar topography of the study area with the location of the studied Ģipka section (black triangle; 22°37′31″E; 57°34′36″N), the location of geological profile A–B and ground penetrating radar (GPR) profile C–D (Fig. 7), Pūrciems (A–F) and Ģipka (A, B) Stone Age settlement sites (black diamonds, detail map with archaeological sites shown in Fig. 8). Locations of the Baltic Ice Lake coastal landforms at elevation 36–32 m a.s.l. (Rosentau *et al.* 2009) and Litorina Sea coastal landforms at elevation 10–9 m a.s.l. (Eberhards 2006) are also shown on the map.

centred around 7.8 cal. ka BP (Rosentau *et al.* 2013; Nirgi *et al.* 2020). In the Rhine–Meuse Delta of the North Sea basin, a major RSL rise event of *c.* 1.9 m has been dated to 8.45 to 8.2 cal. ka BP, while a younger RSL rise event is not evident in the North Sea RSL record (Hijma & Cohen 2019). The end of the rapid melting of the Laurentide and Antarctic ice sheets resulted in a culmination of the Middle Holocene RSL high stand, which in the eastern Gulf of Riga area occurred at *c.* 7.3 cal. ka BP (Rosentau *et al.* 2011; Nirgi *et al.* 2020).

Although there are a few recent detailed RSL studies from the northern, eastern and southern coasts of the Gulf of Riga (Saarse *et al.* 2009; Grudzinska *et al.* 2017; Muru *et al.* 2018; Nirgi *et al.* 2020), there is a lack of comparable data from the western coast of the gulf with a similar uplift history. Our study area in Ģipka, at the western coast of the Gulf of Riga (Fig. 1), is one of the

coastal areas with complex systems of coastal landforms and a palaeolagoon where previous investigations (Grinbergs 1957; Eberhards 2000, 2006) have shown potential for understanding Holocene RSL and GIA variability from the Ancylus Lake to the last marine phase.

In this study, we aimed to reconstruct RSL variability at the Ģipka lagoon, with the main emphases on the Middle Holocene RSL rise, the duration of the high-stand and following decline, as linked to the melting events of the large ice caps and related RSL rise events. We also aimed to provide palaeoenvironmental reconstructions of the Ģipka lagoon system to reconstruct the site preferences of the hunter–gatherer communities that previous archaeological studies have shown were present in the area. The integration of archaeological and palaeoenvironmental records hopefully facilitates

further testing of models of human behavioural–ecological interactions (e.g. at lake or seashores), fundamental for understanding the hunter–gatherer lifeways (Gerasimov & Kriiska 2018; Groß *et al.* 2018). We present here the results of sedimentological, plant macrofossil and diatom analyses with new radiocarbon AMS and optically stimulated luminescence (OSL) ages together with newly available airborne Lidar elevation data, ground penetrating radar (GPR) survey results, and RSL data from the neighbouring areas (Kalniņa & Eberhards 2006; Muru *et al.* 2018).

Geological and archaeological background

The former Litorina Sea lagoon in the Ģipka area, nowadays completely filled in and well drained, is located at the NW coast of the Gulf of Riga in the Irve Plain of the Coastal Lowland (Fig. 1). This slightly undulating plain stretching NW to SE, ~20 km long and up to 1 km wide, at an altitude of 6.4–9.4 m, is isolated from the Baltic Sea by the beach ridge–dune system of the Litorina Sea, reaching altitudes of 14–18 m. To the W and SW, the Ģipka lagoon is bordered by the coastal plains, with Holocene accumulative coastal formations at altitude 12–13 m a.s.l. and coastal formations of the Baltic Ice Lake (32–36 m a.s.l.), located along the eastern slope of the Northern Kursa Upland (Fig. 1C).

The coastal plains fringing the NW coast of the Gulf of Riga are up to 6–7 km wide, and in our study area consist of three rather clear units. The Baltic Ice Lake plain, ~6 km wide, is the most distant from the sea and highest, with a surface altitude ranging from 36 m to 13 m a.s.l. in an EW direction. An accumulative coastal ridge–dune complex above 32 m a.s.l. marks the Baltic Ice Lake shorelines (Fig. 1C). Closer to the sea is the Litorina Sea lagoonal plain, with surface elevations between 9.4 and 6.4 m a.s.l., and the highest point, at 10–9 m a.s.l., marks the highest Litorina Sea (Lit a) coastline along the western edge of the plain (Fig. 1C; Grinbergs 1957; Eberhards 2000, 2006). The lagoonal plain is drained by several SE-flowing meandering streams which have been partially straightened. The river Pilsupe (Fig. 1C), at the bank of which the studied Ģipka outcrop is located, crosses the lagoon in a SW–NE direction and was originally a tributary of the larger river Vecupe and river Roja (Fig. 1C), the latter discharging into the Gulf of Riga in the southern part of the Ģipka lagoon. In *c.* 1885, an artificial channel was dug through the Litorina Sea beach ridge–dune system allowing the river Pilsupe to discharge directly into the Gulf of Riga (Fig. 1C; Nomals 1930). After the channel was dredged in 1926/1927, fluvial erosion accelerated and led to the incision of Pilsupe, resulting in the exposure/outcropping of lagoonal gyttja layers along the banks (Galeniece 1928; Nomals 1930). The currently studied Ģipka outcrop is located in the eastern part of the Ģipka lagoon, at the left bank of the Pilsupe, close to the landward foot of the

beach ridge–dune system of the Litorina Sea (Fig. 1C). This nearly 1-km-wide barrier spit separates the lagoon from the present coastline and represents a ridge–swale complex. According to Kalniņa & Eberhards (2006), this pattern is screened by elongated or parabolic dunes.

The altitude of the bedrock surface of Middle Devonian sandstones ranges from 0 m at the Ancylus Lake highest shoreline down to −15 m a.s.l. at the present coastline (Grinbergs *et al.* 1975; Veinbergs 1996). There is a pronounced scarp in the bedrock surface close to Ancylus Lake highest shoreline, where the bedrock surface altitude falls from 10 to 0 m a.s.l., which is amplified in the modern topography. The thickness of Quaternary cover is ~20 m at the coast, and less than 10 m along the Baltic Ice Lake abrasional plain. The Quaternary strata are composed of thin layers of Late Weichselian till and glaciolacustrine clay, covered mainly by marine and aeolian sandy sediments. Baltic Ice Lake and Ancylus Lake sediments occur only in places on the Irve Plain and reach a total thickness of up to 5 m. The Litorina Sea sandy sediments dominate the marine complex, covered by aeolian sand in the coastal ridge system of the Litorina Sea. An up to 6-m-thick succession of gyttja, buried peat and organic-rich silty or clayey sands has been described in the Ģipka area, associated with the former Litorina Sea lagoon, which is of major interest in the current study (Meirons 1993).

The first biostratigraphic investigation of the Ģipka lagoon sediments was carried out by Galeniece (1928), who first interpreted two gyttja layers separated by fen peat as brackish-water Litorina Sea lagoonal deposits. Grinbergs (1957) and Veinbergs (1996) supported the conclusion about the brackish-water Litorina Sea lagoon by showing that the parallel dune ridge series on top of the barrier spit at the western edge of the Ģipka lagoon represents the highest Litorina Sea coastline (Lit a) at 9.7 m a.s.l. and that two layers of gyttja represent two Litorina Sea transgressive phases with an intermediate lowstand marked by fen peat. It should be noted that neither of these investigations mention a lower fen peat horizon at an altitude *c.* 3 m a.s.l., which was first reported by Grinbergs *et al.* (1975). Grinbergs *et al.* (1975) describes an interval of wood peat containing a large amount of *Betula* pollen (58%), overlying a fine silt and sand horizon. They correlated the peat accumulation with the Yoldia Sea lowstand. Grinbergs *et al.* (1975) also presented the first chronological studies into the Ģipka sediments, giving a conventional radiocarbon age of 8895±85 years (Tln-10) for the lower fen peat and 4440±75 years (Tln-13) for the lower part of the gyttja.

The first archaeological finds at Pūrciems were sherds of Neolithic pottery discovered in 1933 by Burchard and 1937 by Šturms along the actively eroding sand scarp on both sides of the Pilsupe river (Šturms 1937). Six occupation units (dwellings) were discovered, four of them with *in-situ* stratigraphy

(dwellings B–D and F), and another two (A and E) regarded as consisting of redeposited material (Šturms 1937) (Fig. 1C). Later, Loze (2005) re-located dwelling F, where erosion was continuing, and discovered more Neolithic archaeological sites, Ģipka A and Ģipka B (Loze 2005, 2006).

Material and methods

Sediment sampling

Sediment sampling of the 6-m-long Ģipka outcrop on the left bank of the river Pilsupe (22°37′31″E, 57°34′36″N; 7.3 m a.s.l.) (top of the outcrop) was performed in 2017. A series of overlapping 1-m-long monoliths were extracted from the upper 4.5-m-long portion of the vertical succession containing organic matter. Ten-centimetre-diameter U-shaped plastic tubes were pressed into the sediment, cut from the back side and backed into plastic film for the transport. Monoliths were later used for subsampling for biostratigraphy and terrestrial plant macrofossils for further radiocarbon AMS dating.

Three samples for OSL dating were taken from three sand horizons described in the text by hammering 30-cm-long opaque plastic tubes without light exposure. Altogether six ~250 g sand sediment samples were collected from the succession for microtextural properties of mineral grains.

Luminescence dating

The time frame of sand sediment deposition was based on three OSL samples. The sampling tubes were opened under darkroom red subdued light conditions at the Lund Luminescence Laboratory, Sweden. The sediment at each end of the tube was retained for dose rate and water content determination. The sediment from the internal part of the tube was wet sieved, and the 180–250 μm fraction was treated with HCl, H_2O_2 and density separation. In this way, the quartz extracts were obtained and further treated with HF and HCl. Finally, the quartz

extracts were dried and re-sieved on the 180 and 250 μm set of sieves.

High-resolution gamma spectrometers at the Nordic Laboratory for Luminescence Dating, Aarhus University, Denmark were used for measurement (Murray *et al.* 1987), and the final environmental doses were calculated using the DRAC online calculator (Durcan *et al.* 2015).

Considering the proximity to the coast and several submergence–emergence events, average water content was assumed to be similar to the field water content for 50% of the depositional time and saturated for 50% of the time.

To obtain the equivalent dose, large (8 mm) single aliquots of quartz extracts were analysed in a Risø TL/OSL reader DA-20 with a single aliquot regeneration protocol (Murray & Wintle 2000, 2003) preceded by IR/blue ratio, preheating plateau and dose–recovery tests. Blue light sources (470±30 nm; ~65 mW cm^{-2}) and detection through 7 mm of U340 glass filter were used for OSL stimulation. For two samples, 17081 and −82, blue stimulation was used and post-infrared blue stimulation for the sample 17080 (Roberts & Wintle 2001). Equivalent doses (D_e) were calculated in the Risø Analyst 4.31 software. Aliquots were accepted if they revealed a test dose error of <10% (with the exception of sample 17082, where 15% was set), a recycling ratio within 10% of unity (15% for 17082), recuperation <5% of the natural, and for 17080, an IR/B ratio of ≤10%. Between 23 and 30 aliquots per sample were measured, but ~15% of these were rejected owing to poor recycling ratio or dim signals, thus resulting in 21–26 accepted aliquots (Table 1). The Central Age Model was used (Galbraith *et al.* 1999) for final age calculations.

AMS dating and age–depth modelling

Terrestrial plant macrofossils identified during macrofossil analysis were radiocarbon dated using the AMS ^{14}C dating method at Poznan Radiocarbon Laboratory, Poland. Altogether, seven AMS radiocarbon ages were obtained from the Ģipka sediment succession, calibrated

Table 1. List of radiocarbon dates and dated material from the Ģipka section.

Laboratory code	Depth (cm)	^{14}C age (a BP)	Age range (cal. a BP)	Dated material	Comments
Poz-107836	209–210	4145±35	4530–4830	Twigs	Unit G5
Poz-107837	228–230	4155±30	4570–4830	Twigs	Unit G4A
Poz-110080	370–371	6710±40	7500–7670	*Pinus* bark fr., *Pinus* needle fr., *Betula fruits*, *Lycopus europaeus* nutlet, *Scirpus lacustris* fruit	Unit G4A
Poz-107838	392–393	7610±40	8340–8520	*Menyanthes trifoliate* seeds and *Carex* fruits, *Betula* and *Alnus* fruit fr., *Scirpus* fruits	Unit, G3, outliers
Poz-107835	399–400	7820±40	8450–8750	*Pinus sylvestris* needles	Unit G3, outliers
Poz-107869	425–426	7440±40	8170–8360	*Cladium mariscus* fruit fr., *Carex* fruits	Unit G2
Poz-107868	449–450	8120±50	8810–9280	*Pinus* needle fr., *Carex* and *Comarum palustre* fruits	Unit G2

fr = fragment.

using IntCal20 calibration dataset (Reimer *et al.* 2020). The age–depth model was produced using the Oxcal v4.4.4 deposition model by combining AMS radiocarbon dates with a single luminescence date to date the litho- and biostratigraphic boundaries in the Ģipka sequence (Bronk Ramsey 2021).

Wood charcoal samples preserved from the excavation of Neolithic dwellings at Pūrciems in the 1930s were AMS radiocarbon dated at the Laboratory of Mass Spectrometry, Centre for Physical Sciences and Technology, Lithuania, and calibrated as above.

Diatom analysis

In total, 32 samples for diatom analysis were prepared according to the procedure described by Battarbee *et al.* (2001). A drop of the enriched diatom sample was spread over a coverslip, dried overnight at room temperature, and mounted in Naphrax™ (refractive index −1.73) on a microscope slide. The quantitative analyses were performed with a Zeiss Axiophot light microscope under a 100× oil immersion DIC objective. Three samples from the bottommost part of the sediment sequence at the depths 430, 448 and 450 cm were barren of diatoms. In 28 samples, ~230–300 valves (mean count 265 valves per sample) were counted and identified to species level to estimate the relative abundance of taxa. In one sample (at 355 cm) diatom preservation was very poor, and therefore the diatom count was below 200 valves. The diatom identification criteria and ecological information, including salinity preference, were obtained from the Baltic Sea intercalibration guides (Snoeijs 1993; Snoeijs & Vilbaste 1994; Snoeijs & Potapova 1995; Snoeijs & Kasperovičienė 1996; Snoeijs & Balashova 1998) and other well-established diatom floras (Krammer & Lange-Bertalot 1986, 1988, 1991a, b; Witkowski *et al.* 2000; Lange-Bertalot *et al.* 2017) and literature (Denys 1991; van Dam *et al.* 1994), as well as from internet sources (World Register of Marine Species, https://www.marinespecies.org/, and AlgaeBase, Guiry & Guiry 2022). Diatoms were divided into groups according to their salinity tolerance: marine/brackish, halophilous, small fragilarioid taxa with brackish-water affinity, small fragilarioid taxa preferring fresh water, indifferent and freshwater taxa. Diatoms were also classified into groups by their preferred habitat: planktonic and periphytic taxa. Additionally, small fragilarioid taxa as a taxonomically complex and morphologically variable group that can live in benthos, as well as in the water column up to depths of 6–8 m (Brugam *et al.* 1998) as tychoplankton, were separated from periphytic taxa. This is a common practice in diatom studies from isolation basins, since this group is considered to represent pioneer taxa, which are able to adapt to rapid shifts in environmental conditions faster and more effectively than other diatoms (Lotter & Bigler 2000; Yu *et al.* 2004). The predominance of small

fragilarioid taxa is related to environmental instability (Denys 1990) and in isolation basin studies has been observed just prior to, during or after the actual isolation event (Stabell 1985; Heinsalu *et al.* 2000; Risberg *et al.* 2005; Miettinen *et al.* 2007; Saarse *et al.* 2009; Grudzinska *et al.* 2017).

In order to facilitate interpretation of diatom data, stratigraphically constrained incremental sum of squares cluster analysis was performed on the full percentage diatom data to define diatom assemblage zones (DAZ) using Tilia CONISS (Grimm 2011). Detrended correspondence analysis (DCA; Hill & Gauch 1980) with detrending by segments was applied to detect major patterns of variation in the diatom assemblage data during the different development stages of the ancient Ģipka lagoon. Detrended correspondence analysis was used as the diatom data had a gradient 2.7 standard deviation (SD) units long and to avoid an obvious arch effect resulting from the use of principal components analysis (Hill & Gauch 1980; Birks 1995). The DCA was performed using CANOCO 5.1 (after ter Braak & Šmilauer 2018). As DCA is sensitive to rare species, the option in CANOCO 'downweight rare species' was applied. All taxa were square root transformed in order to stabilize the variances and reduce the effects of very abundant taxa (Birks 1995). Lithostratigraphy and diatom data were compiled using the program Tilia v.1.7.16 (Grimm 2011) and compiled in CorelDraw2019.

Plant macrofossil analysis

Altogether, 15 samples were analysed for plant macrofossils. One-centimetre samples with a volume ranging from 100 to 500 mL were collected at different depth intervals between 4.51 and 2.09 m to cover sediment units G2–G5. Preparation for plant macrofossil analysis followed conventional procedures (Birks 2001), using a sieve with 250-µm mesh size. A Zeiss Stemi 2000-C stereomicroscope was used to determine plant macroremains and select the remains of terrestrial plants for ^{14}C AMS dating. Relevant literature and atlases (Katz *et al.* 1965; Cappers *et al.* 2006; Velichkevich & Zastawniak 2006, 2008; Bojnansky & Fargašova 2007) along with a reference collection at the University of Latvia were used for plant macrofossil identification.

Textural properties of the sand

Scanning electron microscope analysis of the microtextural properties of mineral (quartz) grains permits detection of the type of sedimentary environment, namely aeolian, fluvial, glacial and coastal (Mahaney 2002; Smith *et al.* 2018).

To detect this, six sediment samples were taken: one, one and four from the upper (G6), middle (G3), and lower sand (G1), respectively. Samples were air dried and subjected to grain-size analysis using a column of 9–13

sieves (0.063, 0.1, 0.125, 0.18, 0.25, 0.315, 0.5, 0.71, 1.0, 2.0, 4.0, 10.0 and 16.0 mm), depending on the sample. Later, Folk & Ward's (1957) geometric graphical measures, including mean (M), sorting (σ) and skewness (Sk), were calculated. The 0.7–1.0 mm sand fraction was subsampled from the sieve, washed a few times thoroughly in distilled water and dried. Altogether, 120 quartz grains (20 grains per sample) were randomly picked up and processed following the recommendation of Vos *et al.* (2014). Grains were further scanned under a Zeiss EVO MA 15 scanning electron microscope at the Department of Geology, University of Tartu, Estonia using typical magnification in two ranges of: (i) 140–200× for a general grain outline and (ii) 700–1000× for determining the microtextures of the grain surface (Mahaney 2002; Vos *et al.* 2014). Following the latter, the various types of microtextures were semi-quantified based upon the occurrence of microtextures as: abundant (>75%), common (50–74%), moderate (25–49%), sparse (6–24%), rare (<5%) and not observed (0%).

GPR survey

Geophysical studies were carried out using ground penetrating radar (GPR), which offers good data coverage and penetration depth in sandy deposits. The GPR fieldwork was performed with a Zond 12-e double-channel system (Radar System Inc.) using a common-offset configuration with a co-polarized 300 MHz shielded antenna oriented perpendicular to the profile. Similar surveys in the coastal areas of Latvia indicate that 300 MHz antenna is the best compromise between the penetration depth and resolution (Karušs *et al.* 2021; Lamsters *et al.* 2022). The time range for the measurements was 500 ns. A GPR survey was carried out in 2020 along a profile covering 2.2 km perpendicular to the coastline and zones of major coastal landforms (Fig. 1C). The equipment and settings used resulted in clear reflections down to 20 m depth in sandy sediments.

The GPR data were processed and interpreted with Prism 2.61 software. The processing routine included application of time-dependent signal gain function, Ormsby band-pass filter and background removal filter. Conversion from time to a depth scale was performed assuming that characteristic dielectric permittivity is 6, which corresponds to dry sand (Neal 2004). Three boreholes were drilled by hand auger down to a depth of 4.3 m along the GPR profile to verify the interpretation of the obtained reflections. For tracking, a GNSS RTK Emlid Reach RS2 receiver was used, connected to the radar.

Methods for RSL reconstruction

The RSL data from the Ģipka section were used together with the RSL index points from the nearby Ruhnu Island (Muru *et al.* 2018) with similar isostatic uplift to compile a composite RSL curve for the western Gulf of Riga. Vertical and horizontal uncertainties of the RSL data were evaluated using the HOLSEA database format (Hijma *et al.* 2015) and are available in Table S3.

Methods for palaeogeographical modelling

The topographical data for the area around the Ģipka site were provided in the form of a 1 × 1 m resolution Lidar digital terrain model (DTM). Palaeogeographical reconstructions were based on a GIS approach (Rosentau *et al.* 2011), where the palaeosea-level surfaces were subtracted from the DTM.

The palaeosea-level surface for the Litorina Sea maximum stand was interpolated using databases of coastal formations by Saarse *et al.* (2003, 2007). The surface had a vertical error of ±1 m. This was used as a reference surface, and the palaeosea-level surface for 5.5 cal. ka BP was calculated considering a linear decrease in shoreline tilting and the water level taken from the compiled RSL curve based on data from the Ruhnu Island (Muru *et al.* 2018) and the results of the present study. Palaeoshorelines were delineated based on analysis of the elevation and morphology of the coastal ridge–swale complex. Coastal landforms seawards of a palaeoshoreline, younger than the time modelled, were cut by the sea-level surface and then the topography of the whole palaeosea area was generalized to 50 × 50 m resolution and smoothed with a 350 × 350 m averaging filter.

In the Litorina Sea lagoon area, sediments younger than the time modelled were removed from the DTM. A lagoonal sediment body was modelled based on the shape and cross-section of the lagoon and the depth and ages of the sediments recovered from the outcrop at Ģipka site (Fig. 1C). Separate sediment models were created for the time slices 7.3 and 5.5 cal. ka BP (maximum sediment thickness 3.5 and 2.65 m, respectively). In the lagoon area, the river valleys, cutting deep into the lagoonal sediments, were filled up to the level of the surrounding terrain (in general 6 m a.s.l. in the present DTM). Then the DTM was generalized to 10 × 10 m resolution and smoothed with a 50 × 50 m averaging filter to remove noise from modern landscape features inside the lagoon. The respective modelled lagoonal sediment body and the palaeosea-level surface were then subtracted from the modified DTM to create the palaeogeographical reconstruction of the time slice.

Results and interpretation

Sediment stratigraphy and chronology of the Ģipka section

In the sediment stratigraphy of the 6-m-long Ģipka sequence, six sediment units (G1–G6) were defined (Fig. 2): an upwards coarsening sand complex (unit G1), a lower fen peat (unit G2), sand intercalated with
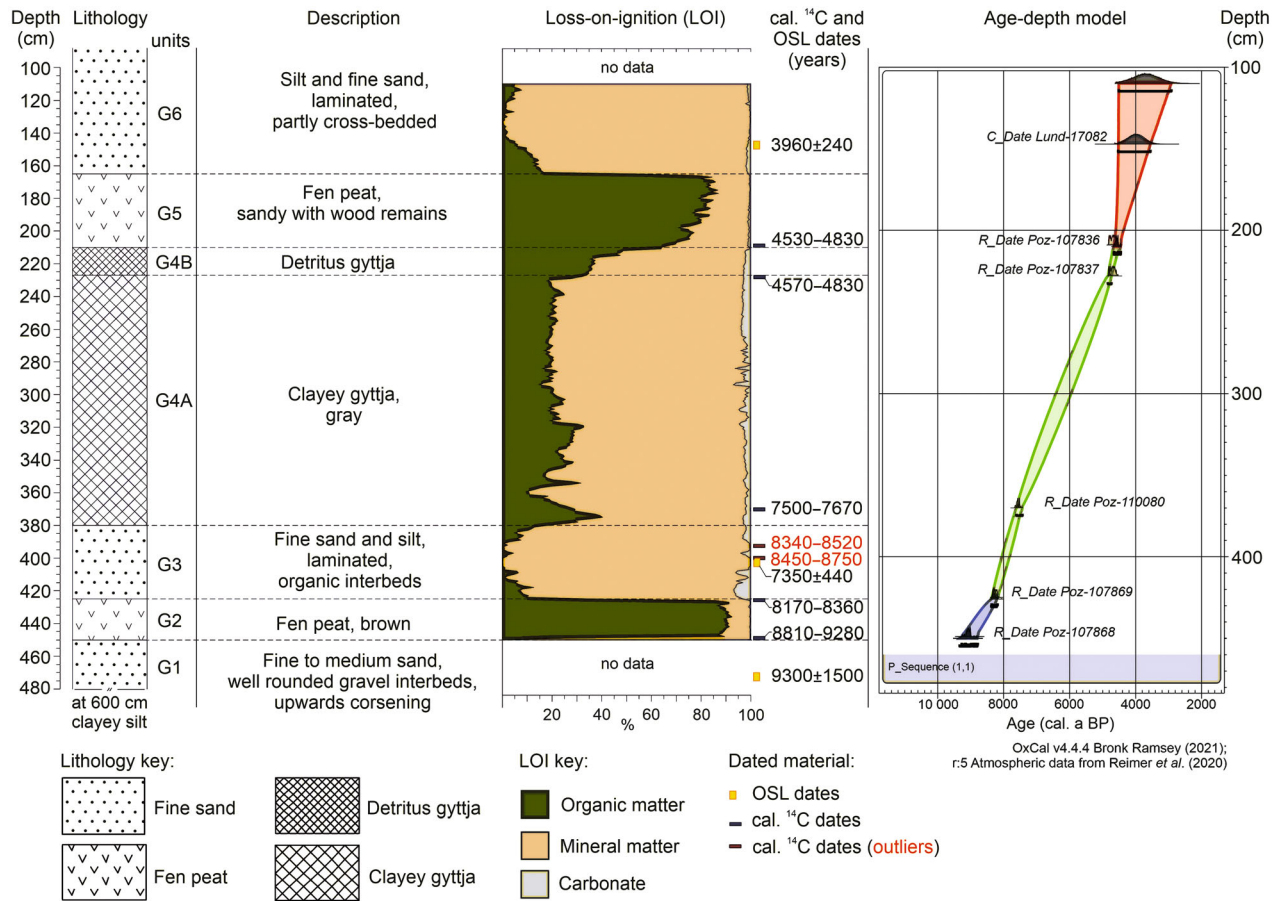
Fig. 2. Stratigraphy and age–depth model of the sediments of the Ģipka section with identified units (G1–G6), loss on ignition and luminescence and radiocarbon ages discussed in the text. For the location of the section see Fig. 1C.

organic matter (OM) lenses (unit G3), clayey gyttja (unit G4A) and detritus gyttja beds (unit G4B) covered by an upper fen peat (unit G5) and organic rich silty-sandy deposits (unit G6).

Altogether, seven AMS radiocarbon dates (Table 1) and three luminescence dates (Table 2) were obtained from this sediment succession. Two radiocarbon dates (Poz-107835 and Poz-107838) from the unit G3 were considered too old compared with the luminescence age from the same unit and compared with AMS dates (Poz-107868 and Poz-107869) from peat layer (G2) below (Fig. 2, Table 1). Dated plant material from the G2 peat succession (Table 1) is considered *in situ* origin as it represents typical fen (dominance of *Carex* spp.) to coastal wetland (a decrease in *Carex* spp. and an increase in aquatic plants – *Cladium mariscus* and *Menyanthes trifoliata*) vegetation, identified using plant macrofossil analyses (Table S2). In contrast, the redeposition of the terrestrial macrofossils (Poz-107835 and Poz-107838) from the former land surface is suspected at the time of the accumulation of G3 sand layer, being the likely reason for older ages of these samples. The final age–depth model is based on five radiocarbon dates and one

luminescence date from the uppermost unit (G6) and covers the main litho- and biostratigraphic boundaries (Fig. 2).

The lowermost unit G1 (interval 600–450 cm) consists of several series of sands, where upward-coarsening alternates with fine to medium beach sand containing well-rounded gravel and pebbles (Fig. 2). Lateglacial clayey silt deposits underlie the G1 unit. Fine sand from the upper part of the unit was OSL dated to *c.* 9.3±1.5 ka. Sediments of the unit G1 are covered by a 25-cm-thick layer (interval 450–425 cm) of well-decomposed dense fen peat (unit G2) with an average OM content of 85% (Fig. 2). According to the age–depth model, the accumulation of this lower fen peat unit in the Ģipka sequence took place between *c.* 9.1 and 8.3 cal. ka BP (Figs 2, 3). The peat is covered by a 25-cm-thick layer of fine sand, containing OM interbeds a few centimetres thick (unit G3), typical for transgressive sands in the coastal area around the Gulf of Riga. Its average OM content is 4%, and the carbonate content is 1–7%, being higher (up to 7%) in the lowermost 15 cm compared with the upper portion (1–2%) of unit G3. According to the age–depth model the deposition of unit G3 took place

Table 2. Summary of radionuclide concentrations, dose rates, water content, equivalent doses and Central Age Model (CAM) ages. s.e. = standard error; *n* = number of quartz aliquots.

Field ID (sample depth, cm)	Laboratory ID Lund	Radionuclide concentration±s.e.			Dose rate±s.e. (Gy ka^{-1})	Water content (%) ±5%	Equivalent dose (Gy)	*n* accepted/ total	CAM age (ka)
		^{232}Th (ppm)	^{238}U (ppm)	^{40}K (ppm)					
G17-3 (150–145)	17082	1.75±0.11	0.88±0.48	1.68±0.05	1.687±0.088	25	6.7±0.2	26/30	3.96±0.24
G17-2 (400–405)	17081	1.57±0.07	0.47±0.19	1.61±0.03	1.558±0.063	24	11.4±0.5	23/23	7.35±0.44
G17-1 (470–475)	17080	1.44±0.25	0.68±1.56	1.46±0.08	1.499±0.220	21	13.7±1.0	21/24	9.3±1.5

between *c*. 8.3 and 7.7 cal. ka BP (Fig. 2). This age range is also confirmed by a single OSL age of *c*. 7.35±0.44 ka, obtained from the middle of unit G3. The sand layer is followed by a 63-cm-thick layer (interval 380–227 cm) of grey clayey gyttja (unit G4A) with an average OM content of 25%. In the lowermost 10 cm, fine sand lenses and peat fragments also occur. According to the age–depth model, deposition of this clayey gyttja took place between *c*. 7.7 and 4.85 cal. ka BP (Fig. 2). The clayey gyttja is overlain by a 17-cm-thick layer (interval 227–210 cm) of brown detritus gyttja (unit G4B) with a much higher OM content (average 38%) compared with unit G4A. According to the age–depth model, its deposition took place between *c*. 4.85 and 4.6 cal. ka BP (Fig. 2). This is followed by accumulation of a 45-cm-thick layer (interval 210–165 cm) of fen peat (unit G5) with an average OM content of 79%. Accumulation of the upper fen peat took place between *c*. 4.6 and 4.2 cal. ka BP and was followed by deposition of a 145-cm-thick layer (interval 165–20 cm) of partly cross-bedded alluvial silt to fine sand (unit G6) with an average OM content of 6%. Fine sand from the lowermost part of unit G6 was OSL dated to *c*. 3.96±0.24 ka (Fig. 2).

Diatom stratigraphy

A 2.73-m-long interval (155–428 cm) of the Ģipka sequence was studied for diatoms. In total, 232 diatom taxa belonging to 70 genera were identified. The relative frequency of the most abundant diatom species is presented in Fig. 3. A table describing the diatom taxa in detail is given in Table S1. The diatom stratigraphy was divided into eight DAZ defined by cluster analysis (CONISS). There are clear changes in the diatom composition, showing a gradual transition from a freshwater to a brackish water environment, and finally isolation and the formation of a shallow lake (Fig. 3).

DAZ-I (428–412 cm; c. 8.4 to 8.1 cal. ka BP). – In the basal sand (unit G1) and fen peat (unit G2) diatoms are not preserved (450–428 cm). The first diatoms, mostly periphytic freshwater and small fragilarioid taxa, appear in the upper part of the fen peat (unit G2) at 428 cm (*c*. 8.4 cal. ka BP), just at the transition from fen peat to grey, silty, fine sand (unit G3). The dominant diatoms are freshwater periphytic *Fragilaria inflata* var. *istvanffyi*

(Pantoscek) Hustedt, *Achnanthidium minutissimum* (Kützing) Czarnecki and indifferent periphytic *Amphora pediculus* (Kützing) Grunow, while small fragilarioid taxa include a high proportion of *Pseudostaurosira brevistriata* (Grunow) D.M.Williams & Round. The diatom composition also includes small fragilarioid taxa that prefer a slightly brackish environment (e.g. *Pseudostaurosiropsis geocollegarum* (Witkowski) E.A.Morales). The first brackish water (e.g. *Fallacia balnearis* (Grunow) A. Witkowski, Lange-Bertalot & Metzeltin and *Diploneis bombus* (Ehrenberg) Ehrenberg) and halophilous diatoms (e.g. *Cocconeis disculus* (Schumann) Cleve) also appear in this zone.

DAZ-II (412–380 cm; c. 8.1 to 7.7 cal. ka BP). – In DAZ-II, marked changes in diatom species composition are observed, where fine sand is intercalated with layers rich in organic matter. In the fine sand, indifferent periphytic (30–51%) diatoms dominate, such as *Psammothidium sp.1*, *Amphora pediculus* and *Karayevia clevei* (Grunow) Bukhtiyarova, whereas in the organic layers the main diatom taxa (40–57%) are freshwater periphytic, such as *Fragilaria inflata* var. *istvanffyi*, *Navicula cari* Ehrenberg and *Navicula antonii* Lange-Bertalot, as well as planktonic *Stephanodiscus alpinus* Hustedt.

DAZ-III (380–356 cm; c. 7.7 to 7.3 cal. ka BP). – DAZ-III starts with a transition from fine sand (unit G3) to grey silty gyttja (unit G4). The dominant species in this zone are small fragilarioid taxa with freshwater affinity (*Pseudostaurosira brevistriata*, *Staurosira venter* (Ehrenberg) Cleve & J.D.Möller, *Staurosira construens* Ehrenberg, *Staurosira binodis* (Ehrenberg) Lange-Bertalot) and towards DAZ-IV the amount of small fragilarioid taxa with brackish-water affinity (e.g. *Nanofrustulum sopotensis* (Witkowski & Lange-Bertalot) E. Morales, C.E.Wetzel & Ector, *Pseudostaurosiropsis geocollegarum*) gradually increases.

DAZ-IV (356–346 cm; c. 7.3 to 7.1 cal. ka BP). – The DAZ-IV is less clearly defined and is distinguished from the underlying DAZ-III only by a decrease in freshwater and an increase in brackish taxa (e.g. *Planothidium delicatulum* (Kützing) Round & Bukhtiyarova, *Planothidium engelbrechtii* (Cholnoky) Round & L. Bukhtiyarova, *Achnanthes fogedii* Håkansson) and the appearance
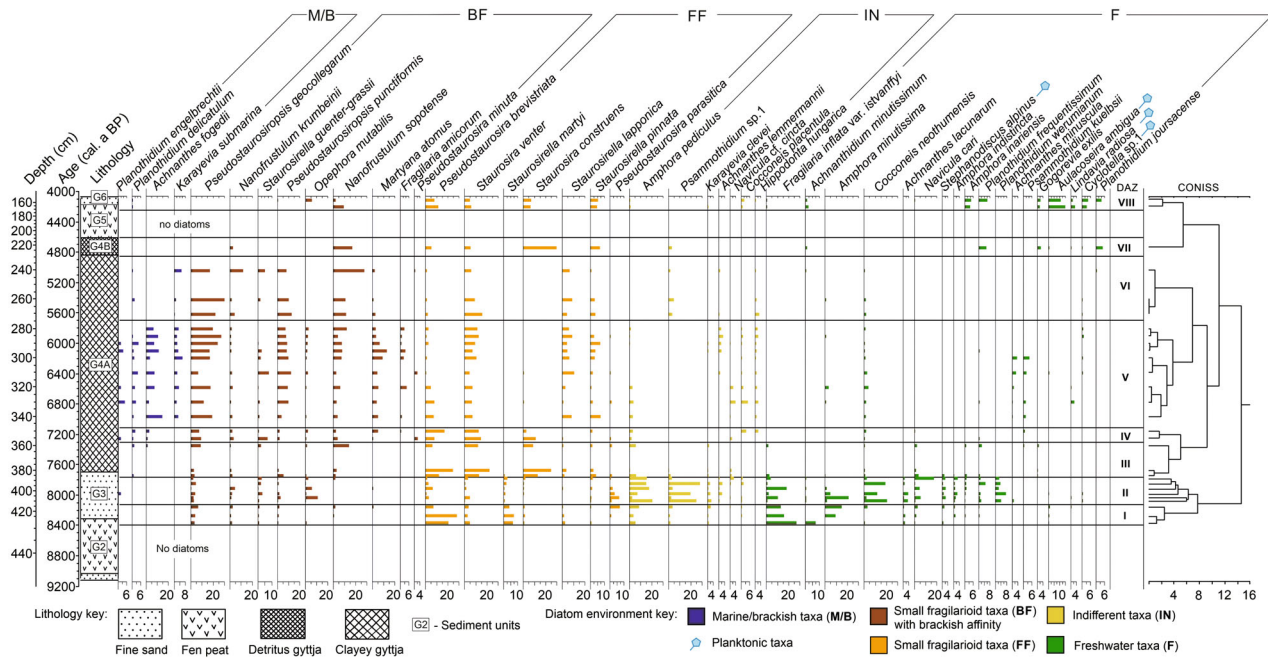
Fig. 3. Percentage diagram of selected (≥2% in two or more samples) diatom taxa from the Ģipka section (arranged according to salinity preference). Diatom assemblage zones (DAZ) are defined by the results of cluster analysis (CONISS).

of halophilous periphytic *Rhoicosphenia abbreviata* (C.Agardh) Lange-Bertalot and planktonic *Cyclotella meneghiniana* (C.Agardh) Lange-Bertalot.

DAZ-V (346–280 cm; c. 7.1 to 5.8 cal. ka BP). – The DAZ-V is characterized by the dominance of small fragilarioid taxa with brackish-water affinity (54%) and significant abundances of marine/brackish (20%) and halophilous (3.5%) diatoms. The most common marine/brackish water diatoms in this zone are *Achnanthes fogedii*, *Karayevia submarina* (Hustedt) Bukhtiyarova, *Planothidium delicatlum* and *P. engelbrechtii*. At the beginning of DAZ-V (6.8 to 6.2 cal. ka BP) an increase in freshwater diatoms is observed (up to 9–11%).

DAZ-VI (280–230 cm; c. 5.8 to 4.8 cal. ka BP). – In DAZ-VI the amount of small fragilarioid taxa with brackish-water affinity gradually increases, reaching a maximum of 71% at 240 cm (*c.* 5.03 cal. ka BP).

DAZ-VII (230–212 cm; c. 4.8 to 4.6 cal. ka BP). – The DAZ-VII is characterized by the replacement of brackish-water-loving small fragilarioid taxa by those preferring freshwater conditions, including *Staurosira construens* (reaching up to 30%), *Pseudostaurosira brevistriata* and *Staurosira pinnata* (Ehrenberg) D.M.Williams & Round, and an increase in periphytic freshwater taxa, such as *Planothidium frequentissimum* (Lange-Bertalot) Lange-Bertalot, *Planothidium joursacense* (Héribaud-Joseph) Lange-Bertalot and *Achnanthidium minutissimum*. Sharp changes in diatom

assemblages were observed together with changes in lithology (clayey gyttja (unit G4A) replaced by detritus gyttja (unit G4B) with higher organic matter content). Subsequently, fen peat at 212–166 cm, which accumulated *c.* 4.6–4.2 cal. ka BP, was barren of diatoms.

DAZ-VIII (166–155 cm; c. 4.2 to 4.0 cal. ka BP). – Although periphytic taxa dominate over planktonic ones in DAZ to VIII, a significant increase in planktonic taxa, such as *Aulacoseira ambigua* (Grunow) Simonsen, *Aulacoseira granulata* (Ehrenberg) Simonsen and *Lindavia radiosa* (Grunow) De Toni & Forti, is recorded. Besides freshwater periphytic diatoms, small fragilarioid taxa, including *Pseudostaurosira brevistriata*, *Staurosira venter*, *Staurosira construens*, *Staurosirella pinnata*, *Nanofrustulum sopotensis* and *Opephora mutabilis* (Grunow) Sabbe & Wyverman, still form a notable part (35–38%) of the diatom composition.

Statistical analyses of the diatom assemblages

The eigenvalues of the first two DCA axes are 0.43 and 0.13, respectively, and together these two axes explain 24% of the cumulative variation within the diatom data (Fig. S1). The first axis scores of DCA showed a gradient length of 2.3 SD units in the diatom assemblages and is plotted against sediment depth (Fig. 4). DCA 1 SD values >2 indicate freshwater conditions (DAZ-I and -II); SD 1.7–1.8, fresh water with slight brackish water influence (DAZ-VII and -VIII); SD 1.3–1.4, transition from fresh water to a brackish environment (DAZ-III);
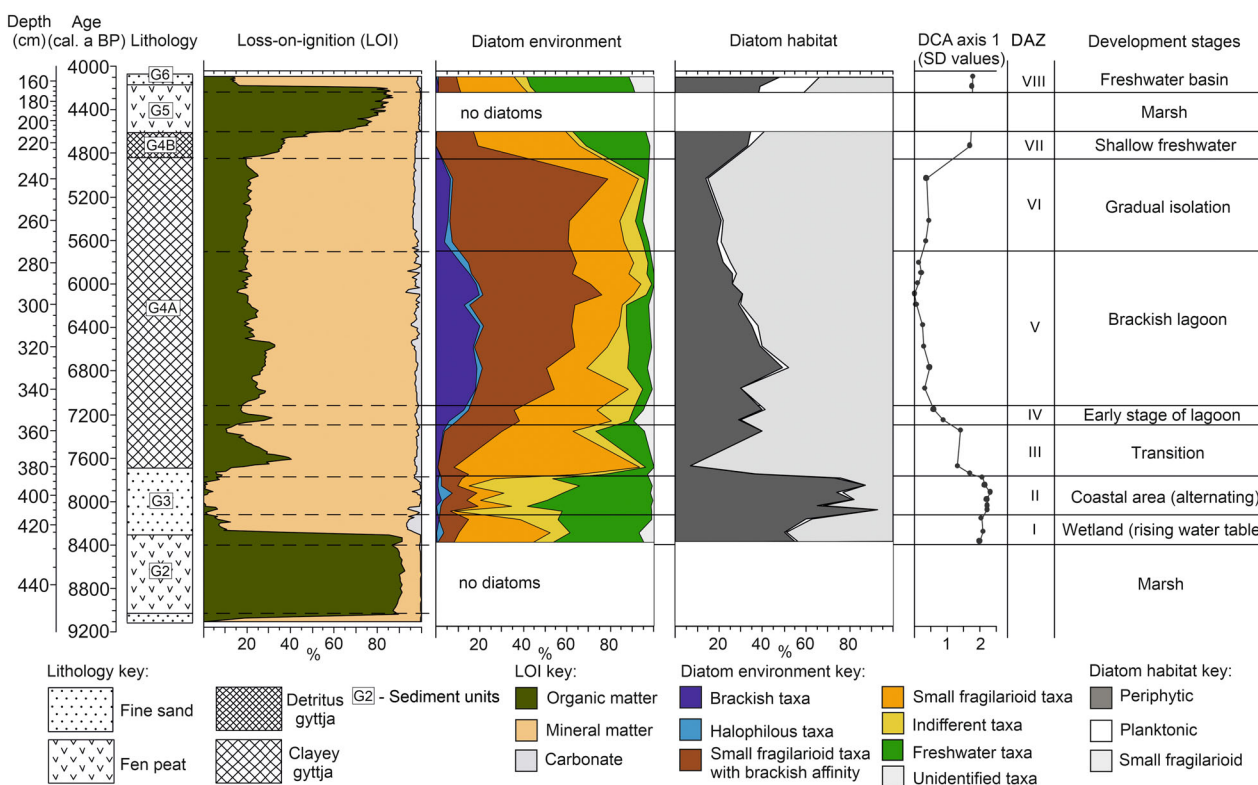
Fig. 4. Summary diagram of lithology, modelled ages, loss-on-ignition (%), diatom distribution based on salinity tolerance and habitat classification (%), DCA 1 showing changes in diatom composition (standard deviation units), and development stages, interpreted based on the description of the lithology, the results of loss on ignition and the changes in diatom composition.

SD 0.6–0.9, a brackish environment with high turbidity (DAZ-IV to -VI); and SD <0.5, a brackish environment (DAZ-V to -VI).

Plant macrofossils

The plant macrofossil taxa from the Ģipka section are given in Table S2. In the lower peat unit (G2) five samples were analysed (Table S2), three of which are from the base and two from the upper portion of the peat, showing a slightly different environment. In the lower part (449–450 cm) well-decomposed dense sandy peat contains detritus predominantly from small plants: rare Hypnales moss leaves and stems, mycorrhizal fungus *Cenococcum geophilum* sclerotia, rounded wood fragments and charcoal, hemp-agrimony (*Eupatorium cannabinum*), rushes (*Juncus*) seeds and *Carex* fruits. This interval is followed by hypnum-grass peat (448–449 cm) dominated by Hypnales leaves of herbaceous plants, *Carex* fruits, rare fruits of wet swampy meadows and fen plants: tormentil (*Potentilla erecta*) and purple marchlocks (*Comarum palustre*). The top part of the peat unit G2 at the transition from medium decomposed fen to silty gyttja (425–427 cm) is rich in Hypnales moss, vascular plant stems, leaf epidermis and aquatic animal chitin fragments. Together with the seeds of white water lily (*Nymphaea alba*), the triple-leaved bogbean *Menyanthes trifoliata* and fruits of great fen sedge (*Cladium mariscus*) occur.

In the overlying sand unit with OM interbeds (G3; 400–396 cm) small, partially rounded flat fragments of wood and charcoal are regularly present, along with mycorrhizal fungus *Cenococcum geophilum* sclerotia, megaspora of *Selaginella selaginoides*, needles of *Pinus sylvestris* and seeds of plants of different habitats (Table S2).

Three samples were analysed from the overlying grey clayey gyttja unit (G4a; 374–371 cm). The remains of aquatic plants dominate: seeds of *Nuphar lutea*, *Nymphaea alba* and *Najas marina*, and fruits of *Ceratophyllum demersum* and *Zannichellia palustris* (Table S2). In addition, the horned pondweed (*Z. palustris*) together with widgeon grass *Ruppia maritima* have previously been described from this sediment unit from the neighbouring borehole 16a (Kalniņa & Eberhards 2006). The horned pondweed prefers a stagnant or slowly flowing water environment – both fresh and brackish water. Following Gessner (1957), *Z. palustris* belongs to a group of polyhaline and mesohaline plants found in waters with highly variable salinity ranging from 35 to 5‰, while widgeon grass prefers a brackish water environment (Gorishina 1979).

Two samples were analysed from the upper portion of the gyttja interval (unit G4B; Table S2). Among the representatives of the aquatic community, fragments of water chestnut *Trapa natans* fruit were found in the lower interval (225–227 cm). Remains of *Stratoites aloides*, *Eleocharis palustris* and *Menyanthes trifoliata* were found in the upper interval (214–215 cm).

Only one sample was analysed from the upper peat unit (G5; 210–209 cm). In this dense wood–grass peat, tree branches with bark, and bark and wood fragments dominate, along with *Alnus glutinosa* and *Betula* sect. Albae fruits and seeds of plants growing in shallow water, *Eleocharis palustris* and *Menyanthes trifoliata*, as well as sedge fruits were found.

Textural and structural properties of sand layers (units G1, G3, G6)

The lower sand horizon (unit G1) reveals semi-horizontal beddings, except for its upper part, where erosional channels are filled with sand of inclined stratification (Fig. 5A) and deformations are found (Fig. 5B). An alternation of finer and coarser fractions up to well-rounded gravel is seen (Fig. 5C) along with an upward fraction coarsening with at least four sequences (Fig. 5D), and dark greyish micaceous-enriched mud rip-up clasts (Fig. 5E). The unit G3 seems structureless (Fig. 5F), whereas G6 unit reveals semi-horizontal beddings (Fig. 5G). Large changes in grain-size parameters are observed in unit G1 (Fig. 6).

Subangular (Fig. S2A) and rounded quartz grains (Fig. S2B) dominate among all investigated sand samples. Angular grains (Fig. S2C) occur only in unit G1 (up to 15%). Among mechanical microtextures, different-sized conchoidal features are common and abundant (>50% of investigated grains, Figs 5, S2D), and enriched with both straight and arcuate steps (Fig. S2E). Crescentic (Fig. S2F) and V-shaped percussion marks (Fig. S2G) occur commonly, except for the grains from G6 unit, where occurrence of these marks is the lowest among all investigated samples. Nearly all grains have precipitation, usually in depressions and holes, and show solution pits on their surface (Fig. S2H). The frequency of chemically induced, oriented etch pits is either sparse or moderate (Fig. S2I,J), but only 7% of grains from unit G3 have such pits on their surface.
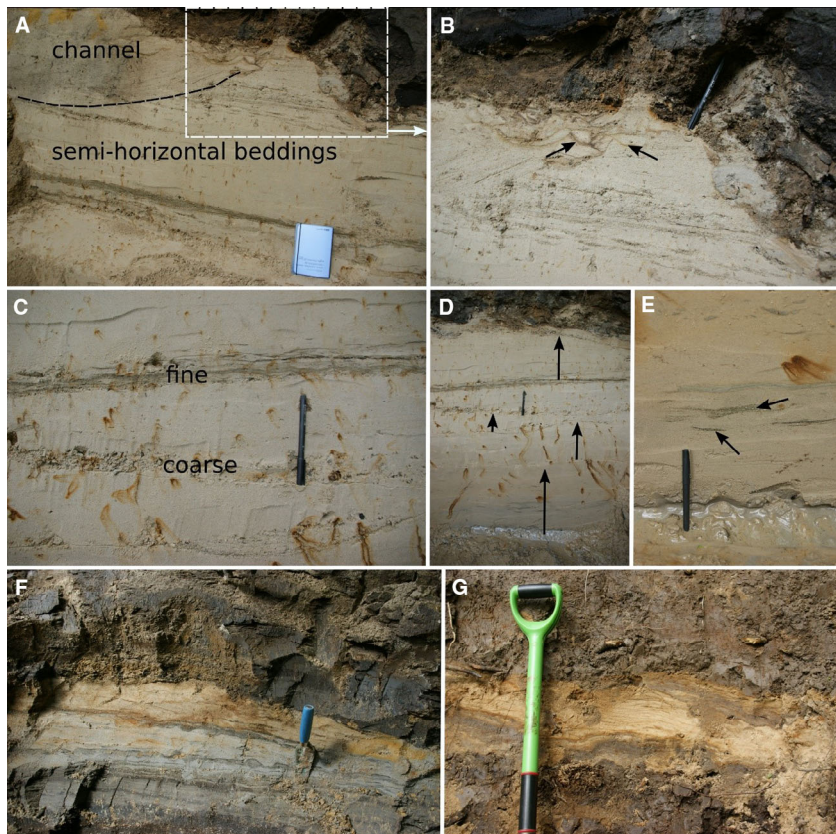

Fig. 5. A. General sediment architecture of the lower sand of the unit G1 (the white square shows deformations in sand as seen in Fig. 6B). B. Deformations (arrows) in the upper part of the lower sand of unit G1 at the contact with the lower fen peat (unit G2). C. Details of alternation of coarser (gravel/pebble) and finer (silt) interlayers. D. Upwards coarsening successions (arrows) in the lower horizon. E. Details of rip-up silt clasts enriched with micaceous minerals. F. Semi-horizontal sand with OM interbeds of the unit G3, with two sets of asymmetric current ripples in the middle of the sand sheet. G. Semi-horizontal sand of the upper horizon (unit G6).
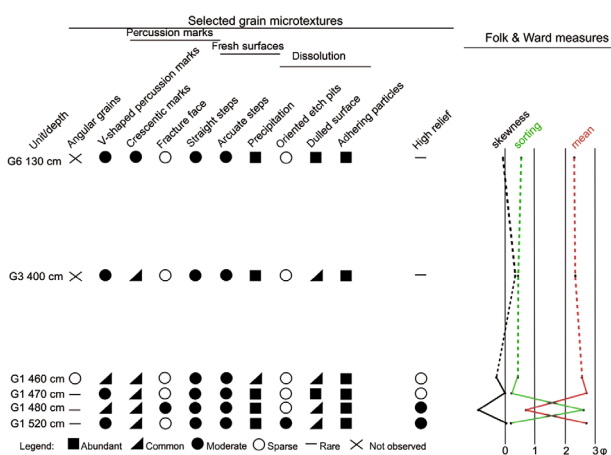
Fig. 6. Selected microtexture frequencies of the investigated quartz grains along with the Folk & Ward (1957) grain-size measures.

Finally, grains are mostly of medium surface relief (Fig. S2K). However, high-relief grains (Fig. S2L) occur moderately and sparsely in G1, and are absent in units G3 and G6.

Palaeoenvironmental interpretation of the Ģipka sediment succession

The palaeoenvironmental interpretation of the Ģipka sediment succession is based on the above-described sediment and diatom stratigraphy, textural and structural properties of the sand units, plant macrofossil results, age–depth modelling based on AMS radiocarbon and luminescence chronology as well as GIS based palaeogeographical reconstruction. Sediment stratigraphy of the Ģipka section is supplemented by newly obtained coring and GPR data along the west–east-oriented cross-section (Fig. 7), which is supplemented by earlier geological data by Eberhards (2003). All this shows a gradual transition from a freshwater coastal environment to a brackish-water environment, followed by isolation of a lagoon and formation of a shallow lake. Such a general trend in palaeoenvironmental change was interrupted by two low-water episodes, when the Ģipka palaeolagoon turned into a wetland, reflected in two fen peat intervals in the studied Ģipka sequence.

Ancylus Lake/Initial Litorina Sea coastal zone (before c. 9.1 cal. ka BP).

– This period corresponds to the lowermost sand horizon (unit G1). Our primary expectation was that this sand complex probably reflects a high-energy coastal environment owing to the coastal site location (Fig. 7A). This assumption is supported by sedimentary structures and the texture of the sand of unit G1. For example, a thick-bedded sand of multiple reversed grading layers, a medium-bedded sand of multiple normal grading layers (Phantuwongraj

et al. 2013) and mud rip-up clasts in a sand matrix (Kempf *et al.* 2017) are interpreted as indicating storm surge washovers. Also, upwards grading layers and mud rip-up clasts occur only in the lower sand (G1) at Ģipka, meaning that this horizon has been affected by past storm action. This is additionally supported by quartz grain surface microtextures (Fig. 6), such as percussion marks, fresh surfaces and others (Costa *et al.* 2012, b). The uppermost part of the coastal sand complex, at elevation 1.3–2.8 m a.s.l. (unit G1), was deposited at *c.* 9.3±1.5 ka, during the Initial Litorina Sea, suggesting that the whole regressive complex occurs at the time when the retreating shoreline of the Ancylus Lake/Initial Litorina Sea passed the Ģipka area. New Lidar elevation data and GPR results show that this nearshore sand complex extended up to 2 km landward from the Ģipka section, forming a well-developed belt of coastal landforms with thick aeolian capping, most probably marking the highest shoreline position of the Ancylus Lake (Fig. 7). Fine grained clayey–silty deposits were described in core B3 (Fig. 8), behind these coastal landforms, suggesting the existence of an Ancylus Lake lagoon. We interpret GPR reflector 1 as the surface of the glacial till rising below the Ancylus Lake coastal landform up to the elevation 7 m a.s.l. and reflector 2 up to the elevation 13 m a.s.l. as the contact between Ancylus Lake coastal sands and aeolian capping.

Coastal fen (c. 9.1 to 8.4 cal. ka BP).

– This period corresponds to the major part of the lower fen peat layer (unit G2). The onset of the lower peat accumulation at *c.* 9.1 cal. ka BP shows that RSL dropped below 3 m a.s.l. during the regression and that fen peat accumulation in the coastal depression at Ģipka started soon after the water level decrease in the study area. The occurrence of plant macrofossils of coastal wetland habitats, such as *Menyanthes trifoliata*, *Cladium mariscus*, *Juncus*, *Carex* and *Eupatorium cannabinum* (Table S2), suggests fen formation in a coastal area that was probably also seasonally flooded, as suggested by the presence of mineral matter in the peat layer (Fig. 2).

Transition from fen to coastal wetland (c. 8.4 to 8.1 cal. ka BP).

– This period corresponds to the uppermost part of the lower peat layer (unit G2) and the lowermost part of the sand layer (unit G3) of DAZ-I (Fig. 3). In the uppermost 3 cm of the peat, the first diatoms appear, showing a transition from fen to coastal wetland owing to the rising water table at *c.* 8.4 cal. ka BP, as derived from our age–depth modelling. The diatom composition suggests a freshwater environment, but also includes small fragilarioid taxa preferring a slightly brackish environment, which might be an indication of seawater intrusion. Also, the abundance of macrofossils of various aquatic plants, such as *Nymphaea alba*, *Cladium mariscus*, *Potamogeton*, *Scirpus lacustris*, *Menyanthes trifoliata*, *Batrachium* and *Myriophyllum verticillatum*
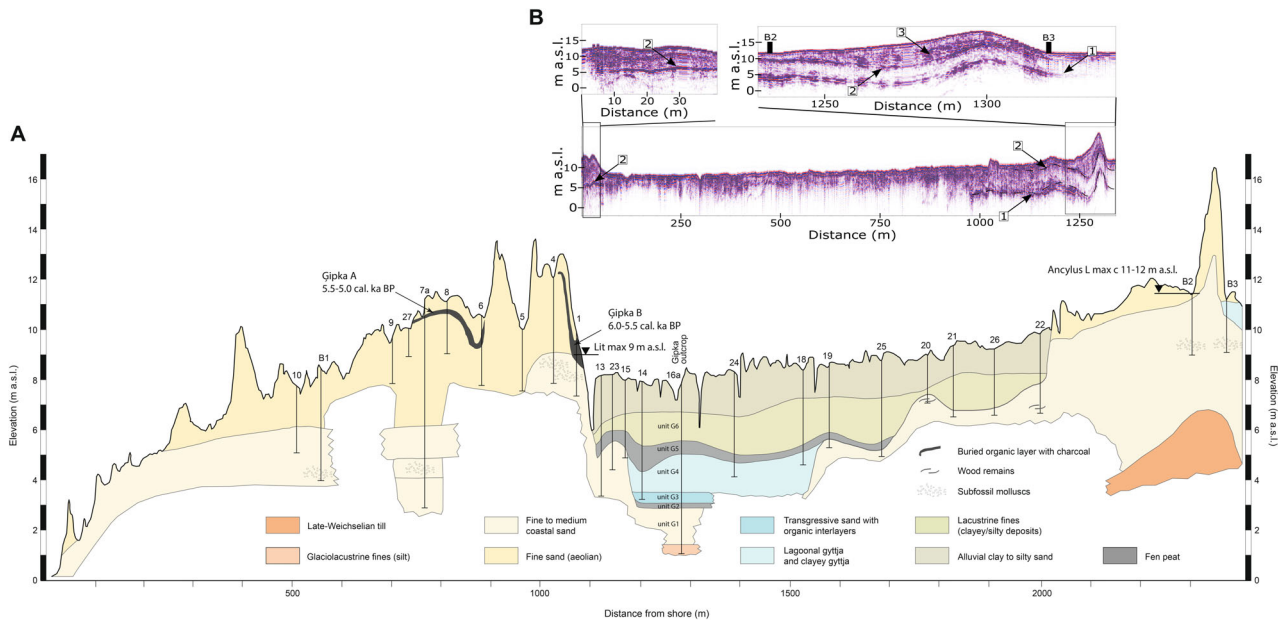
Fig. 7. A. Geological cross-section through the Ģipka basin, based on coring data by Eberhards (2003), some new studied sediment sections (Ģipka outcrop; cores B1–B3) and interpretation of Lidar and GPR data. B. GPR images of the section crossing the Ģipka basin. Numbers show the most prominent GPR reflectors described in the text. We interpret reflector 1 as the surface of the glacial till rising below the Ancylus Lake coastal landform up to the elevation 7 m a.s.l. and reflector 2 as the contact between Ancylus Lake coastal sands and aeolian capping. Internal reflector 3 is interpreted as a layering of a dune. The locations of the geological cross-section (A–B) and GPR image (C–D) are given in Fig. 1C.

along with *Carex* (Table S2), is characteristic for this environment. Changes in lithology from sandy peat accumulation to fine sand deposition with redeposited OM interbeds are interpreted as marking the beginning of the marine transgression in the Ģipka area.

Shallow-water coastal estuary (c. 8.1 to 7.7 cal. ka BP). – This period corresponds to the major part of the sand layer with OM interbeds (unit G3) in DAZ-II (Fig. 3). Rapid changes in diatom assemblages along with alternating mineral and organic-rich sediment layers suggest a highly variable environment, as in an estuary with a strong interplay between sea-level rise and freshwater discharge from a river. Also, the similar composition of the plant taxa compared with the underlying unit G2 indicates probable redeposition owing to activation of erosional processes along the Ģipka basin.

The fine sand of unit G3 lacks angular quartz grains, and this combines with the rare occurrence of high-relief grains. These features distinguish this horizon from the sands of unit G1 and, combined with rather stable grain-size properties (mean, sorting, skewness) and (semi-)horizontal/cross-bedding, argue for an environment of lower energy, rather than intense storm action. In coastal environments subangular to rounded grains with silica precipitation and enriched with oriented etch pits and V-shaped percussion cracks are likely (Krinsley & Doornkamp 1973; Mahaney 2002; Kalińska-Nartiša *et al.* 2017; Itamiya *et al.* 2019; Martewicz *et al.* 2022), and this description largely coincides with the outline of

the investigated grains, except for the subangular shapes. The sand horizon yielded a number of subrounded and rounded grains almost without high relief, but instead with dulled surfaces covered with V-shaped marks. These latter marks develop in fluvial transport (Lindé & Mycielska-Dowgiałło 1980), probably suggesting mixed conditions during the deposition of G3 sand, with both fluvial and wave influence (moderate oriented etch pitting). The presence of asymmetric current ripples in G3 sands also supports this conclusion (Fig. 5F).

Coastal lagoon (c. 7.7 to 4.8 cal. ka BP). – This period corresponds to the uppermost part of the sand layer with OM interbeds (unit G3) and the clayey gyttja layer (unit G4A) in DAZ-III to -VI (Fig. 3). A high degree of environmental instability with mass occurrence of fragilarioid taxa coupled with the occurrence of some broken parts of the strongly brackish-tolerant *Campylodiscus clypeus* (Ehrenberg) Ehrenberg ex Kützing and *C. echeneis* Ehrenberg ex Kützing at *c.* 7.7 to 7.3 cal. ka BP (DAZ-III) is recorded. This, along with plant macrofossils typical of the transgressive phase of the Litorina Sea, such as seeds of *Najas marina*, *Zannichellia palustris* and *Ceratophyllum demersum* (Yu *et al.* 2004), is interpreted as a result of the quickly rising sea-level and onset of lagoon formation owing to development of the coastal barrier in the area NE of the Ģipka section. Nearshore sands together with subfossils of *Cerastoderma edule*, *Macoma baltica*, *Mytilus edulis* (Meirons 1993), *Peringia ulvae* and *Ecrobia ventrosa* (pers. comm. M. Rudzīte) are seen up to an elevation of
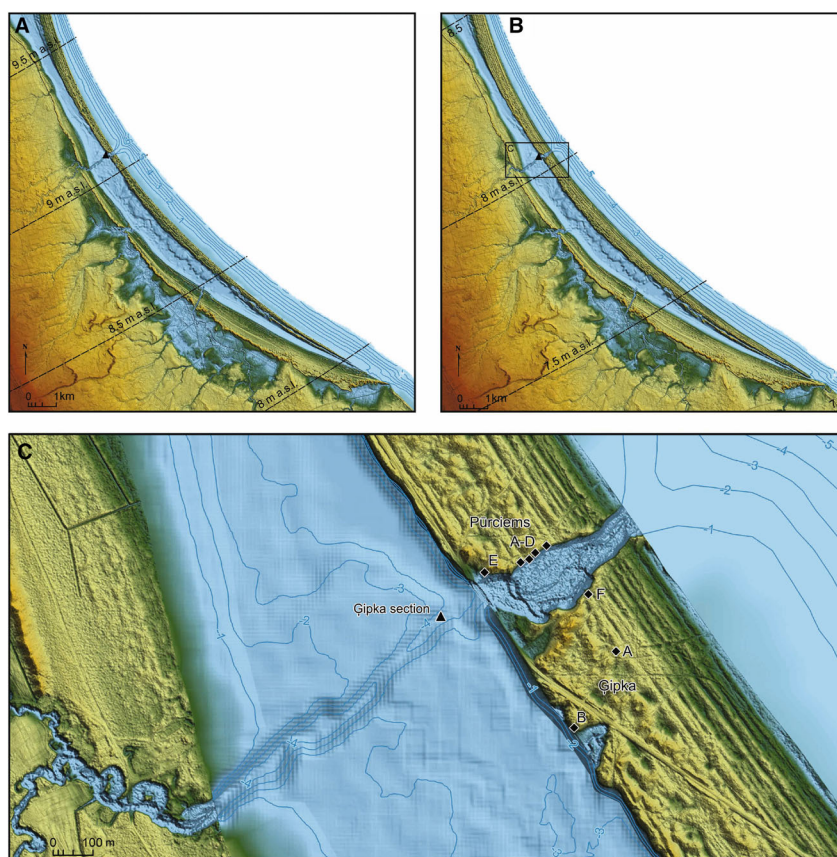
Fig. 8. Palaeogeographical reconstructions of the development of the Ģipka area with RSL isobases. A. Litorina Sea lagoon during the RSL highstand at *c*. 7.3 cal. ka BP. B. Litorina Sea lagoon at *c*. 5.5 cal. ka BP and during the Neolithic occupation. C. Detail of the lagoon and its possible passage at 5.5 cal. ka BP with the location of the Pūrciems (A–F) and Ģipka (A, B) settlement sites and studied Ģipka section.

~9 m a.s.l. within the barrier deposits, covered by ~3 m (max. 8 m) of aeolian sand (Fig. 7A).

This quickly rising RSL period in the Ģipka record is followed by a gradual increase in brackish and halophilous diatom taxa and the establishment phase of the brackish lagoon at *c*. 7.3 to 7.1 cal. ka BP (DAZ-IV). The brackish periphytic diatoms represented by *Karayevia submarina*, *Planothidium delicatlum* and *P. engelbrechtii*, including *Achnanthes fogedii*, recorded as a typical fossil taxon in the Litorina Sea sediments (Snoeijs & Kasperovičienė 1996; Witkowski *et al*. 2000; Grudzinska *et al*. 2014), suggest the existence of the Ģipka brackish lagoon, with the strongest influence of the Litorina Sea between *c*. 7.1 and 5.8 cal. ka BP (DAZ-V) and the highest salinities *c*. 6.1 cal. ka BP (Fig. 4). At the same time the strongest marine water intrusions were observed in Lake Lilaste in the southern part of the Gulf of Riga (Grudzinska *et al*. 2017).

In previous studies (Seppä *et al*. 2000; Risberg *et al*. 2005; Grudzinska *et al*. 2012, 2013), mass abundance of small fragilarioid taxa, which are considered as pioneer species with the ability to cope successfully with rapid changes in salinity and turbidity (Yu *et al*. 2004), was interpreted as a sign of the isolation.

Hence, the dominance of *Pseudostaurosiropsis geocollegarum*, *Pseudostaurosiropsis punctiformis* (Witkowski, Metzeltin & Lange-Bertalot) Witkowski, Seddon & Pliński and *Nanofrustulum sopotensis*, coupled with a noticeable decline in brackish periphytic diatoms, for a millennium-long period between *c*. 5.8 and 4.8 cal. ka BP (DAZ-VI), following our age–depth modelling, indicates slow and gradual isolation of the lagoon, most probably owing to the gradual lowering of the RSL.

Freshwater coastal lake (c. 4.8 to 4.6 cal. ka BP) with possible intermittent brackish water inflows. – This period corresponds to the detritus gyttja layer (unit G4B) and DAZ-VII (Fig. 3). The diatom composition shows a distinct freshening of the environment, characterized by the replacement of small fragilarioid taxa that prefer brackish water by species preferring freshwater conditions. The presence of *Nanofrustulum sopotensis* and *N. krumbeinii* in the lake can be explained by the higher electrical conductivity that remained after isolation, although it cannot be excluded that the lake had a small connection to the Gulf of Riga into which brackish water may have occasionally inflowed owing to stronger easterly winds. This, together with the abundance of the

macrofossils of various aquatic and coastal plants, suggests the existence of a shallow eutrophic coastal lake (Table S2). The main water supply during this period was most probably from the rivers and streams entering the lake. The water level in the coastal lake was regressive and most probably controlled by falling RSL, finally leading to overgrowing of the lake, which started at *c.* 4.6 cal. ka BP.

Coastal fen (c. 4.6 to 4.2 cal. ka BP). – This period corresponds to the upper fen peat (unit G5), which is barren of diatoms. The plant macrofossil assemblage (Table S2) suggests a coastal peatland which was probably also seasonally flooded, as indicated by the presence of mineral matter in the peat. Gradually increasing OM content upwards in the peat and disappearance of aquatic plants indicate drier conditions in the later phase of fen development.

River floodplain with coastal lakes (since c. 4.2 cal. ka BP). – This period corresponds to the upper sand and silt interval (unit G6) in DAZ-VIII (Fig. 3). In the geological cross-section this period is characterized by various subaqueous and terrestrial sediment layers, interpreted as a floodplain deposit, including small local lakes, swamps and channel deposits (Fig. 7). The lowermost part of the floodplain deposit is represented in the Ģipka section by laminated fine sand with OM containing freshwater periphytic diatoms and small fragilarioid taxa, suggesting at least periodic existence of isolated freshwater lakes in the floodplain. Subrounded and rounded sand grains almost without high relief but instead with dulled surfaces and covered with V-shaped marks suggest fluvial transport of grains and therefore strong river input into the lake.

Archaeological chronology and location of Neolithic sites

The earliest evidence of human settlement is from Ģipka B, located on the landward side of the Litorina Sea dune belt at 9 m a.s.l. (Fig. 8; Loze 2006). The assemblage of Comb Ware pottery indicates occupation *c.* 6.0 to 5.5 cal. ka BP; organic-tempered pottery has been recovered too, showing that the site was also used during the time interval *c.* 5.5 to 5.0 cal. ka BP. This is typical for western Latvia: there is very little evidence of coastal settlement before *c.* 6 cal. ka BP, with abundant remains from *c.* 6–5 cal. ka BP, and once again a paucity of evidence for coastal occupation after *c.* 5 cal. ka BP.

All of the other Neolithic sites/dwellings (Pūrciems A–F and Ģipka A) are located within the dune belt at elevations of 9–13 m a.s.l., archaeological stratigraphy taking the form of thin occupation layers in the dune sands (Figs 8, 9). These occupations have likewise yielded finished and semi-manufactured amber ornaments, and are known in particular for the finds of clay figurines and associated evidence of 'ritual' activities involving ochre

(Šturms 1937; Loze 2005, 2006). The five new AMS radiocarbon dates obtained for Pūrciems dwellings C, D and F span the period *c.* 5.6 to 5.0 cal. BP (Table S4), and the characteristics of the pottery from the other Pūrciems dwellings and the Ģipka A site indicate occupation approximately during the same period (Bērziņš 2008; Lõugas & Bērziņš 2023).

Discussion

Ancylus Lake development in the western Gulf of Riga

An unresolved issue in the postglacial development of the west coast of the Gulf of Riga is the maximum water level and extent of the Ancylus Lake. Our luminescence date from the uppermost part of the high energy nearshore sand complex (unit G1) suggests that at *c.* 9.3±1.5 ka the retreating coastline of the Ancylus Lake/Initial Litorina Sea passed the Ģipka area, as visible from the storm footprints recorded in the lower sand unit (G1). GPR results combined with Lidar elevation data show that this sand complex extends up to 2 km landward from the studied Ģipka section, forming at its landward limit a belt of coastal landforms at an elevation of 11–13 m a.s.l., covered by aeolian sands (Fig. 7). This NW–SE oriented concave belt of coastal formations can be observed for at least 30 km and probably marks the maximum extent of the Ancylus Lake (Fig. 1C), thus contradicting the earlier interpretation by Grinbergs (1957), who considered these to be Litorina Sea formations. The elevation of the Ancylus Lake highest shoreline at Ģipka (ridge foot at 11–12 m a.s.l.; Fig. 7) is also similar to the elevation of the Ancylus Lake maximum (13 m a.s.l.) mapped in the Pärnu area (Saarse *et al.* 2003), eastern Gulf of Riga, with a similar uplift rate, where it is dated to *c.* 10.2 cal. ka BP (Nirgi *et al.* 2020). Deposition at similar time frame between *c.* 10.2 and 10.82 ka is also known from western Latvian coast in the ancient Ventspils lagoon (Kalińska *et al.* 2022). Later, during the lake regression, a series of shore-parallel sandy coastal ridges (Fig. 1C) were formed seaward of the Ancylus Lake highest shoreline, as seen in the geological profile, partly buried under younger lagoonal and alluvial deposits (Fig. 7). The formation of a series of storm-induced ridges at gradually lower altitude supports the continuous outflow scenario of the Ancylus Lake after its highstand, convincingly documented in the southern Kattegat (Bendixen *et al.* 2017).

RSL changes in the western Gulf of Riga during the Litorina Sea

The lower fen peat (unit G2) accumulation on top of the coastal sands suggests low RSL (below 3 m a.s.l.) during the Initial Litorina Sea from *c.* 9.1 cal. ka BP (Fig. 9). Data from the Ģipka succession do not provide information about the lowest RSL, but it is likely that
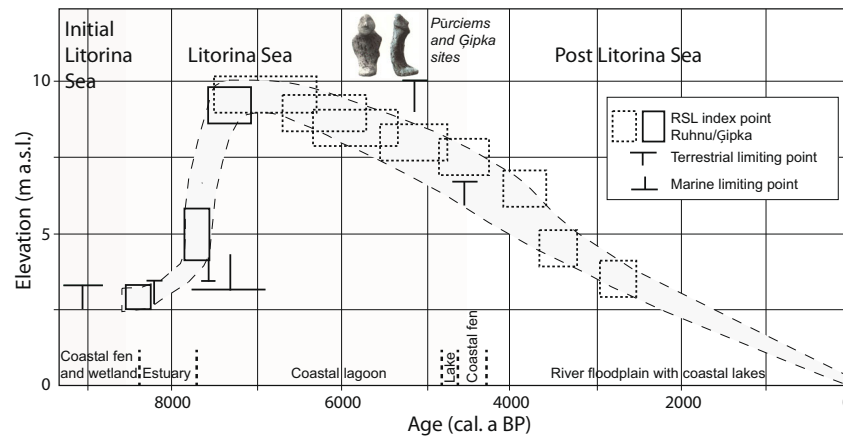
Fig. 9. Composite RSL curve for the western Gulf of Riga combining RSL index points from Ruhnu Island (Muru *et al.* 2018) and RSL data from the Ģipka area. Environmental changes in the Ģipka area are presented at the bottom and Baltic development stages (after Andrén *et al.* 2011) at the top of the graph. For the locations of the sites see Fig. 1. The RSL data in HOLSEA database format are presented in Table S3. Clay figurine from the Pūrciems site associated with 'ritual' activities involving ochre (Šturms 1937) marks the habitation period between 6.0 and 5.0 cal. ka BP.

RSL dropped close to or even below the present sea-level, as there is evidence of RSL below the present level at that time in the Pärnu area in the eastern Gulf of Riga owing to a similar uplift history (Fig. 1; Nirgi *et al.* 2020). Based on AMS radiocarbon-dated terrestrial macrofossils in tandem with the onset of unit G3 accumulation, the subsequent arrival of fresh to slightly brackish transgressional waters at Ģipka is dated to *c.* 8.4 cal. ka BP (Table S3). After initial flooding of the area, wave and fluvial-influenced shallow-water estuary sediments with interbeds of redeposited terrestrial organic matter accumulated around 8.1 to 7.7 cal. ka BP with an estimated RSL at Ģipka *c.* 4–6 m a.s.l. (Fig. 9). Lithological changes from the accumulation of shallow water sand (G3) towards lagoonal gyttja clay (G4a) accumulation and changes in diatom composition at *c.* 7.7 cal. ka BP (Fig. 4; Table S3) mark the ongoing rise in RSL and the formation and growth of the barrier in front of the lagoon. The rising RSL period in the Ģipka record is followed by the establishment phase of the brackish lagoon at *c.* 7.3 to 7.1 cal. ka BP and probably marks the culmination of the Litorina Sea transgression at the mapped marine limit of the coastal barrier at elevation *c.* 9 m a.s.l. (Fig. 7; Table S3). Following our RSL reconstruction, during the initial period of transgression, between *c.* 8.4 and 7.7 cal. ka BP, the water level rise was slower, around 2 m, compared with a subsequent sea-level rise of 4 m from *c.* 7.7 cal. ka BP until the culmination of the transgression at *c.* 7.3 cal. ka BP (Fig. 9).

Possible causes of the RSL change and comparison with other RSL reconstructions

The onset of the transgression at Ģipka concurs with the age of the major RSL rise event detected in different locations around the globe (Li *et al.* 2012; Amorosi *et al.* 2013; Wang *et al.* 2013; Lawrence *et al.* 2016) and dated in high precision in the Rhine–Meuse Delta (North Sea) to between 8.45 and 8.2 cal. ka BP (Hijma & Cohen 2019). This about 1.9 m RSL rise event (Hijma & Cohen 2019) is related to the rapid melting of the Laurentide Ice Sheet and drainage of the glacial lake Agassiz–Ojibway *c.* 8.5 to 8.2 cal. ka BP (Lajeunesse & St-Onge 2008). In the BSB, this event probably initiated the onset of a brackish-water phase in Femern Belt (Bennike *et al.* 2022), a 1–2 m transgression (L1) accompanied by relatively low salinity, in the Blekinge area (Berglund *et al.* 2005) and the onset of the Litorina Sea transgression in the slowly uplifting Västervik–Gamlebyviken (Katrantsiotis *et al.* 2022), Narva–Luga (Rosentau *et al.* 2013), Pärnu (Nirgi *et al.* 2020) and western Gulf of Riga areas around 8.5 to 8.4 cal. ka BP. Despite somewhat different uplift rates (Fig. 1A), these areas experienced almost simultaneous RSL rise, probably owing to the rapid nature of sea-level rise.

The second transgression (L2) in Blekinge (Berglund *et al.* 2005) seems to be the most prominent period of RSL rise, centred around 7.8 to 7.6 cal. ka BP and documented in the western Gulf of Riga, as well as in many areas around the BSB (Yu *et al.* 2007; Rosentau *et al.* 2013; Sander *et al.* 2015; Nirgi *et al.* 2020). It is interesting that the rapid sea-level rise at 7.8 to 7.6 cal. ka BP is not detected in the high-resolution RSL data from the Rhine–Meuse Delta. On the one hand, it may suggest regional RSL phenomena related to GIA processes (collapsing forebulge; García-Artola *et al.* 2018); on the other hand, it may relate to the interpretation of the Rhine–Meuse data.

The culmination of the Litorina Sea transgression at elevation 9 m a.s.l. in the western Gulf of Riga around *c.* 7.3–7.1 cal. ka BP (Fig. 9) is consistent with the end of the final melting of the Laurentide Ice Sheet *c.* 7.0 cal. ka BP

and a significant slow-down in global sea-level rise starting from *c*. 6.7 cal. ka BP (Lambeck *et al.* 2014). Thus, after *c*. 7 cal. ka BP the rate of postglacial uplift in our study area exceeded the rate of global sea-level rise (Fig. 9).

RSL and salinity changes in the lagoon

The percentage of brackish and marine diatoms in the Ģipka lagoon shows the strongest influence of the Litorina Sea at about 1000 years after the RSL high-stand (Fig. 9), between *c*. 7.1 and 5.8 cal. ka BP, with the highest seawater salinities around 6.1 cal. ka BP (Figs 4, S1). This delay probably reflects the regional salinity changes in BSB related to the ongoing widening of the straits at Öresund and Great Belt in combination with decreased freshwater supply to the BSB owing to the climate shift (Gustafsson & Westman 2002; Andrén *et al.* 2011; Ning *et al.* 2017). The study by Gustafsson & Westman (2002) also shows that freshwater input into the BSB was 15–60% lower than present during the maximal salinity phase around 6 cal. ka BP and showed a salinity decrease during the subsequent millennia, agreeing with our results.

Development of the Ģipka lagoon and Neolithic hunter–gatherers

Neolithic hunter–gatherer groups in Ģipka and Pūrciems settled in the sandy grounds on top of the Litorina Sea barrier system, preferring the landward side of the system (Ģipka A and Pūrciems A–D) and the lagoon shores (Ģipka B and Pūrciems E) (Fig. 8). The valley-like depression in historical topographic maps from the beginning of the twentieth century (Karte des westlichen Russlands 1914–1919) may indicate that somewhere between sites Pūrciems D and F a passage to the lagoon also may have existed (Fig. 8), although owing to later human-induced disturbances (dredging of the channel) during the twentieth century (Nomals 1930), this morphological evidence is inconclusive.

Settlements between seashore and lagoon may be regarded as a typical locus of Neolithic settlement in the sandy coastal belt along the southern and western shores of the Gulf of Riga. Thus, sites from the same period have been discovered in the sandy belts separating the former lagoons and coastal lakes in the region (Bērziņš *et al.* 2016, 2022a). The Ģipka–Pūrciems sites, occupied *c*. 6–5 cal. ka BP, are concentrated at the deepest, seaward side of the lagoon with water depths up to 3–4 m (Fig. 8C). Salinity reconstructions show that during the occupation the lagoon was a brackish water body with high productivity and calm waters, and therefore probably well suited for the installation of fishing constructions, as at the Priedaine site (Fig. 1B) at the shore of a concurrent palaeolake at the head of the Gulf of Riga.

The faunal remains from neighbouring Siliņupe and Priedaine (Fig. 1B; Bērziņš *et al.* 2016, 2022b) indicate that sites at the shore of lagoons and coastal lakes could also serve as bases for hunting trips to catch terrestrial mammals, probably because the waters offered good transport connections along the coastal belt and with the hinterland. It is evidently not fortuitous that the Ģipka–Pūrciems concentration of sites is located directly opposite the mouth of the Pilsupe river, entering the lagoon from the landward side (Fig. 8C): this waterway would have connected the coastal community with inland areas, important for access to resources and for contact with inland groups. Hence, the Pūrciems–Ģipka locality may be regarded not only as a very attractive location for hunting and fishing in the Stone Age, but also as a node of transport and communications.

The Ģipka B site, by the shore of the lagoon, has produced the earliest evidence of occupation. Following our palaeogeographical reconstructions, the open sea was less than 0.5 km distant, and it may be that conditions on the narrow dune belt were too inhospitable for settlement. Subsequently, occupation did spread to the dune belt itself, and this area also had a particular social and religious significance – as seen from the evidence of activities involving the application of powdered ochre and the fragmentation of clay figurines (Fig. 9; Loze 2005). The Pūrciems–Ģipka area evidently lost its particular attractiveness as a settlement locus along with terrestrialisation of the former lagoon and lake from *c*. 4.6 cal. ka BP.

Conclusions

- The Ancylus Lake highest shoreline was formed in the Ģipka area at an elevation of *c*. 11–12 m a.s.l., reaching an elevation ~2 m higher and located ~2 km landward of the highest shoreline of the Litorina Sea. During the regression of the Ancylus Lake/Initial Litorina Sea, a series of shore-parallel coastal landforms, today buried under younger sediments, were formed before *c*. 9.3±1.5 ka, when the regressive coastline passed the study area at Ģipka.

- A new RSL curve for the western Gulf of Riga has been constructed based on the RSL data from the Ģipka area and from the nearby Ruhnu Island. The reconstruction shows that the last marine transgression in the western Gulf of Riga started at *c*. 8.4 cal. ka BP and concurred with the 1.9 m RSL rise event between 8.45 and 8.2 cal. ka BP recorded from the North Sea basin. Owing to the rapid nature of the sea-level rise, it caused almost simultaneous transgression in BSB areas with different postglacial land uplift rates. Most of the RSL rise in the western Gulf of Riga occurred later, between *c*. 8.2 and 7.3 cal. ka BP, followed by RSL fall owing to the significant slow-

down in global sea-level rise and ongoing postglacial land uplift.

- New diatom, plant macrofossil, textural and structural sediment properties and chronological data from the Gipka section show the development of the Gipka area in connection with the RSL changes, with the following stages: open coast with regressive Ancylus Lake/Initial Litorina Sea coastline before *c.* 9.1 cal. ka BP, coastal fen (*c.* 9.1–8.4 cal. ka BP) and wetland (*c.* 8.4–8.1 cal. ka BP), estuary (*c.* 8.1–7.7 cal. ka BP), Litorina Sea lagoon (*c.* 7.7–4.8 cal. ka BP), freshwater coastal lake (*c.* 4.8–4.6 cal. ka BP), fen (*c.* 4.6–4.2 cal. ka BP) and river floodplain (since *c.* 4.2 cal. ka BP).

- During the existence of the lagoon, settlement sites of Neolithic hunter–gatherer groups were established on the shores of the lagoon in the period *c.* 6.0–5.0 cal. ka BP. Salinity reconstructions based on diatom assemblages show that during the occupation the lagoon was a brackish waterbody with high productivity and calm waters. The Gipka–Pūrciems Stone Age settlement concentration occupied a particularly advantageous location: directly opposite the mouth of the Pilsupe River, which would have served as a pathway connecting the coastal communities with territories further inland, thus facilitating access to resources and contact with inland groups. The Pūrciems–Gipka area evidently lost its particular attractiveness as a settlement locus along with terrestrialisation of the lake from *c.* 4.6 cal. ka BP.

Author contributions. – AR prepared the manuscript with comments and contributions from all co-authors and compiled the age–depth model, RSL database and RSL curve. IG performed the diatom analyses and interpretation and prepared the diatom diagrams. EK analysed the textural properties of sand layers. HA performed the luminescence dating and interpretation of results. VB provided archaeological chronology and interpretation. AC and LK performed plant macrofossil analysis. JK and KL made GPR survey and data interpretation. MM compiled palaeogeographical reconstructions and overview maps. LP made loss on ignition analyses. AR, TH, EK, MN, AC did the fieldwork and sediment sampling.

Data availability statement. – The data that support the findings of this study are openly available in the Supporting Information.

References

Amorosi, A., Rossi, V. & Vella, C. 2013: Stepwise post-glacial transgression in the Rhone Delta area as revealed by high-resolution core data. *Palaeogeography, Palaeoclimatology, Palaeoecology 374*, 314–326.

Andrén, T., Björck, S., Andrén, E., Conley, D., Zillén, L. & Anjar, J. 2011: The development of the Baltic Sea Basin during the last 130 ka. *In* Harff, J., Björck, S. & Hoth, P. (eds.): *The Baltic Sea Basin*, 75–97. Springer, Heidelberg, Dordrecht, Berlin, New York.

Battarbee, R., Jones, V. J., Flower, R. J., Cameron, N. G., Bennion, H., Carvalho, L. & Juggins, S. 2001: Diatoms. *In* Smol, J. P., Birks, H. J. B. & Last, W. (eds.): *Tracking Environmental Change Using Lake Sediments, Volume 3: Terrestrial, Algal, and Siliceous Indicator*, 155–202. Kluwer Academic Publishers, Dordrecht.

Bendixen, C., Jensen, J. B., Boldreel, L. O., Clausen, O. R., Bennike, O., Seidenkrantz, M.-S., Nyberg, J. & Hübscher, C. 2017: The Holocene Great Belt connection to the southern Kattegat, Scandinavia: Ancylus Lake drainage and Early Littorina Sea transgression. *Boreas 46*, 53–68.

Bennike, O. & Jensen, J. B. 2013: Postglacial relative shore level changes in Lillebælt, Denmark. *Geological Survey of Denmark and Greenland Bulletin 28*, 17–20.

Bennike, O., Philippsen, B., Groß, D. & Jessen, C. 2022: Holocene shore-level changes, southern Lolland and the Femern Belt, Denmark. *Journal of Quaternary Science 38*, 440–451.

Berglund, B. E., Sandgren, P., Barnekow, L., Hannon, G., Jiang, H., Skog, G. & Yu, S.-Y. 2005: Early Holocene history of the Baltic Sea, as reflected in coastal sediments in Blekinge, southeastern Sweden. *Quaternary International 130*, 111–139.

Bērziņš, V. 2008: *Sārnate: Living by a Coastal Lake during the East Baltic Neolithic*. 473 pp. University of Oulu, Oulu. Available at: http://herkules.oulu.fi/isbn9789514289415/isbn9789514289415.pdf.

Bērziņš, V., Breijers, E., Kalińska, E. & Krievāns, M. 2022a: Shifting shores and Stone Age settlement: the Former Ventspils Lagoon area, Latvia. *Environmental Archaeology*, https://doi.org/10.1080/14614103.2022.2136819.

Bērziņš, V., Čakare, A., Kalniņš, M., Lõugas, L., Mīlgrāve, I. & Zagorska, I. 2022b: Amber wind and porpoise jaw: resource use at Siliņupe (fourth mill. BC) on the Baltic's Gulf of Riga Coast. *The Journal of Island and Coastal Archaeology*, https://doi.org/10.1080/15564894.2022.2125127.

Bērziņš, V., Ceriņa, A., Kalniņš, M., Lõugas, L., Lübke, H. & Meadows, J. 2016: Priedaine: a Neolithic site at the head of the Gulf of Riga. *Archaeologia Baltica 23*, 12–37.

Birks, H. J. B. 1995: Quantitative palaeoenvironmental reconstructions. *In* Maddy, D. & Brew, S. (eds.): *Statistical Modelling of Quaternary Science Data*, 161–254. Quaternary Research Association, Cambridge.

Birks, H. H. 2001: Plant macrofossils. *In* Smol, J. P., Birks, H. J. B. & Last, W. M. (eds.): *Tracking Environmental Change Using Lake Sediments, Volume 3: Terrestrial, Algal, and Siliceous Indicator*, 49–74. Kluwer Academic Publishers, Dordrecht.

Bojnansky, Y. V. & Fargašova, A. 2007: *Atlas of Seeds and Fruits of Central and East-European Flora*. 1046 pp. Springer Netherlands, Dordrecht.

ter Braak, C. J. F. & Šmilauer, P. 2018: *Canoco Reference Manual and User's Guide: Software for Ordination (Version 5.10)*. 536 pp. Microcomputer Power, Ithaca.

Bronk Ramsey, C. 2021: OxCal 4.4 Manual. Available at: https://c14.arch.ox.ac.uk/.

Brugam, R. B., McKeever, K. & Kolesa, L. 1998: A diatom-inferred water depth reconstruction for an Upper Peninsula, Michigan, lake. *Journal of Paleolimnonolgy 20*, 267–276.

Cappers, R. T. J., Bekker, R. M. & Jans, J. E. A. 2006: *Digital Seed Atlas of The Netherlands*. Barkhus Publishing & Groningen University Library, Groningen.

Costa, P. J. M., Andrade, C., Dawson, A. G., Mahaney, W. C., Freitas, M. C., Paris, R. & Taborda, R. 2012: Microtextural characteristics of quartz grains transported and deposited by tsunamis and storms. *Sedimentary Geology 275–276*, 55–69.

Costa, P., Andrade, C., Freitas, M., Oliveira, M., Lopes, V., Dawson, A., Moreno, J., Fatela, F. & Jouanneau, J.-M. 2012: A tsunami record in the sedimentary archive of the central Algarve coast, Portugal: characterizing sediment, reconstructing sources and inundation paths. *The Holocene 22*, 899–914.

van Dam, H., Mertens, A. & Sinkeldam, J. 1994: A coded checklist and ecological indicator values of freshwater diatoms from The Netherlands. *Netherlands Journal of Aquatic Ecology 28*, 117–133.

Denys, L. 1990: *Fragilaria* blooms in the Holocene of the western coastal plain of Belgium. *In* Simmola, H. (ed.): *Proceedings of the 10th International Diatom Symposium*, 397–406. Koenigstein, Koeltz and Biopress, Bristol.

Denys, L. 1991: A check-list of the diatoms in the Holocene deposits of the western Belgian coastal plain with a survey of their apparent ecological requirements, vol II. Professional Paper. Geological Survey of Belgium, 1991-03(247), 92 pp.

Durcan, J. A., King, G. E. & Duller, G. A. T. 2015: DRAC: Dose Rate and Age Calculator for trapped charge dating. *Quaternary Geochronology 28*, 54–61.

Eberhards, G. 2000: Rīgas līča Kurzemes ziemeļu piekrastes Litorīnas jūras krasta veidojumi un akmens laikmeta apdzīvotības rašanās ģeoloģiskās vides apstākļi [Coastal formations and geological conditions of formation of the Stone Age settlement of the Litorina Sea, northern coast of the Gulf of Riga Kurzeme]. *Arheoloģija un etnogrāfija 20*, 211–222.

Eberhards, G. 2003: *Latvijas jūras krasti [Latvian sea coasts]*. 259 pp. Latvijas Universitāte, Riga.

Eberhards, G. 2006: Pūrciema apkārtnes reljefs, ģeoloģiskā uzbūve un attīstība [Relief, geological structure and development of the Pūrciems area]. *In* Loze, I. (ed.): *Neolithic Dune Settlements in Northern Kurzeme*, 12–28. Institute of the History of Latvia, Riga.

Feldens, P. & Schwarzer, K. 2012: The Ancylus Lake stage of the Baltic Sea in Fehmarn Belt: indications of a new threshold? *Continental Shelf Research 35*, 43–52.

Folk, R. L. & Ward, W. C. 1957: Brazos River bar: a study in the significance of grain size parameters. *Journal of Sedimentary Petrology 27*, 3–26.

Galbraith, R. F., Roberts, R. G., Laslett, G. M., Yoshida, H. & Olley, J. M. 1999: Optical dating of single and multiple grains of quartz from Jinmium rock shelter, Northern Australia: Part I, Experimental design and statistical models. *Archaeometry 41*, 339–364.

Galeniece, M. 1928: Divas jaunas fosīlas *Trapa natans* atradnes Latvijā [New localities with fossil *Trapa natans* in Latvia]. *Acta Horti Botanici Universitatis Latviensis 3*, 95–102.

García-Artola, A., Stephan, P., Cearreta, A., Kopp, R., Khan, N. & Horton, B. 2018: Holocene sea-level database from the Atlantic coast of Europe. *Quaternary Science Reviews 196*, 177–192.

Gerasimov, D. & Kriiska, A. 2018: Early-Middle Holocene archaeological periodization and environmental changes in the Eastern Gulf of Finland: interpretative correlation. *Quaternary International 465*, 298–313.

Gessner, F. 1957: *Meer und Strand*. 426 pp. Deutscher Verlag der Wissenschaften, Berlin.

Gorishina, T. K. 1979: *Plant Ecology*. 368 pp. Vishaja Shkola, Moscow.

Grimm, E. 2011: *Tilia Software v. 1.7.16*. Illinois-State-Museum. Research and Collection Center, Springfield.

Grinbergs, E. 1957: *The Late Glacial and Postglacial History of the Coast of the Latvian SSR*. 122 pp. The Publishing House of the Academy of Sciences of the Latvian SSR, Riga.

Grinbergs, E. F., Kessel, H. J., Punning, J. M. K. & Rajamäe, R. M. 1975: Application of radiocarbon method to study ancient Baltic transgressions in Latvia. *In* Afanasijev, G. D. (ed.): *State of Methodological Research in Absolute Geochronology*, 182–186. Nauka, Moscow.

Groß, D., Zander, A., Boethius, A., Dreibrodt, S., Grøn, O., Hansson, A., Jessen, C., Koivisto, S., Larsson, L., Lübke, H. & Nilsson, B. 2018: People, lakes and seashores: studies from the Baltic Sea basin and adjacent areas in the early and mid-Holocene. *Quaternary Science Reviews 185*, 27–40.

Grudzinska, I., Saarse, L., Vassiljev, J. & Heinsalu, A. 2013: Mid- and late-Holocene shoreline changes along the southern coast in of the Gulf of Finland. *Bulletin of the Geological Society of Finland 85*, 19–34.

Grudzinska, I., Saarse, L., Vassiljev, J. & Heinsalu, A. 2014: Biostratigraphy, shoreline changes and origin of the Limnea Sea lagoons in northern Estonia: the case study of Lake Harku. *Baltica 27*, 15–24.

Grudzinska, I., Saarse, L., Vassiljev, J., Heinsalu, A. & Veski, S. 2012: A palaeocoastline reconstruction for the Käsmu and Pärispea peninsulas (northern Estonia) over the last 4000 years. *Estonian Journal of Earth Sciences 61*, 307–316.

Grudzinska, I., Vassiljev, J., Saarse, L., Reitalu, T. & Veski, S. 2017: Past environmental change and seawater intrusion into coastal Lake Lilaste, Latvia. *Journal of Paleolimnology 57*, 257–271.

Guiry, M. D. & Guiry, G. M. 2022: *AlgaeBase*. World-wide electronic publication, National University of Ireland, Galway. Available at: https://www.algaebase.org (accessed 17.01.2022).

Gustafsson, B. G. & Westman, P. 2002: On the causes for salinity variations in the Baltic Sea for the last 8500 years. *Paleoceanography 17*, 1–14.

Hansson, A., Nilsson, B. & Sjöström, A. 2018: A submerged Mesolithic lagoonal landscape in the Baltic Sea southeastern Sweden – Early Holocene environmental reconstruction and shore-level displacement based on a multiproxy approach. *Quaternary International 463*, 110–123.

Heinsalu, A., Kohonen, T. & Winterhalter, B. 2000: Early post-glacial environmental changes in the western Gulf of Finland based on diatom and lithostratigraphy of sediment core B–51. *Baltica 13*, 51–60.

Hijma, M. & Cohen, K. 2019: Holocene sea-level database for the Rhine-Meuse Delta, The Netherlands: implications for the pre-8.2 ka sea-level jump. *Quaternary Science Reviews 214*, 68–86.

Hijma, M. P., Engelhart, S. E., Törnqvist, T. E., Horton, B. P., Hu, P. & Hill, D. F. 2015: A protocol for a geological sea-level database. *In* Shennan, I., Long, A. J. & Horton, B. P. (eds.): *Handbook of Sea-Level Research*, 536–553. Wiley Blackwell, Oxford.

Hill, M. O. & Gauch, H. G. 1980: Detrended correspondence analysis – an improved ordination technique. *Vegetatio 42*, 47–58.

Itamiya, H., Sugita, R. & Sugai, T. 2019: Analysis of the surface microtextures and morphologies of beach quartz grains in Japan and implications for provenance. *Progress in Earth and Planetary Science 6*, 43, https://doi.org/10.1186/s40645-019-0287-9.

Kalińska, E., Breijers, E., Alexanderson, H., Krievāns, M. & Bērziņš, V. 2022: A chronology of depositional coastal landforms of the Baltic Sea: luminescence dating of sandy sediments and patterns of human settlement at the ancient Ventspils Lagoon. *Estuarine, Coastal and Shelf Science 279*, 108135, https://doi.org/10.1016/j.ecss.2022.108135.

Kalińska-Nartiša, E., Alexanderson, H., Nartišs, M., Stevic, M. & Kaiser, K. 2017: Sedimentary features reveal transport paths for Holocene sediments on the Kristianstad coastal plain, SE Sweden. *GFF 139*, 147–161.

Kalniņa, L. & Eberhards, G. 2006: Stop 6: morphology, geological structure and development of the Ģipka lagoon. *In* Stinkulis, Ģ. & Zelčs, V. (eds.): *The Baltic Sea Geology: The Ninth Marine Geological Conference. Pre-Conference and Post-Conference Field Excursion Guidebook*, 39–44. University of Latvia, Riga.

Karte des westlichen Russlands 1914–1919. Available at: https://vesture.dodies.lv/#m=15/57.58107/22.63377&l=O/KDW.

Karušs, J., Lamsters, K., Poršņovs, D., Zandersons, V. & Ješkins, J. 2021: Geophysical mapping of residual pollution at the remediated Inčukalns acid tar lagoon, Latvia. *Estonian Journal of Earth Sciences 70*, 140–151.

Katrantsiotis, C., Dahl, M., Palm, V., Rönnby, J., Andrén, T. & Andrén, E. 2022: Holocene relative sea level changes in the Västervik-Gamlebyviken region on the southeast coast of Sweden, southern Baltic Sea. *Boreas 52*, 206–222.

Katz, N., Katz, S. & Kipiani, M. 1965: *Atlas and Keys of Fruits and Seeds Occurring in the Quaternary Deposits of the U.S.S.R.* 364 pp. Nauka, Moscow.

Kempf, P., Moernaut, J., Van Daele, M., Vandoorne, W., Pino, M., Urrutia, R. & De Batist, M. 2017: Coastal lake sediments reveal 5500 years of tsunami history in south central Chile. *Quaternary Science Reviews 161*, 99–116.

Krammer, K. & Lange-Bertalot, H. 1986: Bacillariophyceae 1. Teil Naviculaceae. *In* Ettl, H., Gerloff, J., Heying, H. & Mollenhauser, D.

(eds.): *Süsswasserflora von Mitteleuropa*, vol. *2/1*, 876 pp. Gustav Fisher Verlag, Stuttgart.

Krammer, K. & Lange-Bertalot, H. 1988: Bacillariophyaceae 2. Teil Bacillariaceae, Epithemiaceae, Surirellaceae. *In* Ettl, H., Gerloff, J., Heying, H. & Mollenhauser, D. (eds.): *Süsswasserflora von Mitteleuropa*, vol. *2/2*, 596 pp. Gustav Fisher Verlag, Stuttgart.

Krammer, K. & Lange-Bertalot, H. 1991a: Bacillariophyaceae 3. Teil Centrales, Fragilariceae, Eunotiaceae. *In* Ettl, H., Gerloff, J., Heying, H. & Mollenhauser, D. (eds.): *Süsswasserflora von Mitteleuropa 2/3*, 576 pp. Gustav Fisher Verlag, Stuttgart.

Krammer, K. & Lange-Bertalot, H. 1991b: Bacillariophyaceae 4. Teil Achnanthaceae. *In* Ettl, H., Gerloff, J., Heying, H. & Mollenhauser, D. (eds.): *Süsswasserflora von Mitteleuropa 2/4*, 437 pp. Gustav Fisher Verlag, Stuttgart.

Krinsley, D. H. & Doornkamp, J. C. 1973: *Atlas of Quartz Sand Surface Textures.* 91 pp. Cambridge University Press, Cambridge.

Lajeunesse, P. & St-Onge, G. 2008: The subglacial origin of the Lake Agassiz-Ojibway final outburst flood. *Nature Geoscience 1*, 184–188.

Lambeck, K., Rouby, H., Purcell, A., Sun, Y. & Sambridge, M. 2014: Sea level and global ice volumes from the last glacial maximum to the Holocene. *Proceedings of the National Academy of Sciences of the United States of America 111*, 15296–15303.

Lambeck, K., Smither, C. & Johnston, P. 1998: Sea-level change, glacial rebound and mantle viscosity for northern Europe. *Geophysical Journal International 134*, 102–144.

Lamsters, K., Karušs, J., Stūrmane, A., Ješkins, J. & Džeriņš, P. 2022: Mapping of large-scale diapir structures at the paleo-ice tongue bed in western Latvia from geophysical investigations and borehole data. *Quaternary International 630*, 3–16.

Lange-Bertalot, H., Hofmann, G., Werum, M. & Cantonati, M. 2017: Freshwater benthic diatoms of Central Europe: over 800 common species used in ecological assessment. *In* Cantonati, M., Kelly, M. G. & Lange-Bertalot, H. (eds.): *English Edition with Updated Taxonomy and Added Species*, 942 pp. Koeltz Botanical Books, Oberreifenberg.

Lawrence, T., Long, A. J., Gehrels, W. R., Jackson, L. P. & Smith, D. E. 2016: Relative sea-level data from southwest Scotland constrain meltwater-driven sea-level jumps prior to the 8.2 kyr BP event. *Quaternary Science Reviews 151*, 292–308.

Li, Y.-X., Törnqvist, T. E., Nevitt, J. M. & Kohl, B. 2012: Synchronizing a sea-level jump, final Lake Agassiz drainage, and abrupt cooling 8200 years ago. *Earth and Planetary Science Letters 315–316*, 41–50.

Lindé, K. & Mycielska-Dowgiałło, E. 1980: Some experimentally produced microtextures on grain surfaces of quartz sand. *Geografiska Annaler: Series A, Physical Geography 62*, 171–184.

Lotter, A. F. & Bigler, C. 2000: Do diatoms in the Swiss Alps reflect the length of ice-cover? *Aquatic Sciences 62*, 125–141.

Lõugas, L. & Bērziņš, V. 2023: Natural history and exploitation of the harbor porpoise (Phocoena phocoena Linnaeus, 1758) during the Neolithic (ca. 4000–2000 cal. BC) in the Eastern Baltic Region. *Animals 13*, 909, https://doi.org/10.3390/ani13050909.

Loze, I. 2005: Small anthropomorphic figurines in clay at Ģipka Neolithic settlements. *Documenta Praehistorica 32*, 155–165.

Loze, I. 2006: *Neolīta apmetnes Ziemeļkurzemes kāpās [Neolithic Dune Settlements in Northern Kurzeme]*. 223 pp. Latvijas vēstures institūta, Rīga.

Mahaney, W. C. 2002: *Atlas of Sand Grain Surface, Textures and Applications.* 256 pp. Oxford University Press, Oxford.

Martewicz, J., Kalińska, E. & Weckwerth, P. 2022: What hides in the beach sand? A multiproxy approach and new textural code to recognition of beach evolution on the southern and eastern Baltic Sea coast. *Sedimentary Geology 435*, 106154, https://doi.org/10.1016/j.sedgeo.2022.106154.

Meirons, Z. 1993: Quaternary deposits. *In* Tracevsky, G. (ed.): *Results of Geological Mapping at Scale 1:50,000 on the Territory of Latvia (Map Sheets 0–34-81-B, G, 0–34-82-B, 0–34-93-A,B,C,G, 0–34-95-B, 0–34-105-A,B, 0–34-106-A,C (Talsi, Kolka))*, 191–199. Report 11035 in Latvian State Geological Archive, Riga.

Miettinen, A. 2004: Holocene Sea-level changes and glacio-isostasy in the Gulf of Finland, Baltic Sea. *Quaternary International 120*, 91–104.

Miettinen, A., Savelieva, L., Subetto, D. A., Dzhinoridze, R., Arslanov, K. & Hyvärinen, H. 2007: Palaeoenvironment of the Karelian Isthmus, the easternmost part of the Gulf of Finland, during the Litorina Sea stage of the Baltic Sea history. *Boreas 36*, 441–458.

Murray, A. S. & Wintle, A. G. 2000: Luminescence dating of quartz using an improved single-aliquot regenerative-dose protocol. *Radiation Measurements 32*, 57–73.

Murray, A. S. & Wintle, A. G. 2003: The single aliquot regenerative dose protocol: potential for improvements in reliability. *Radiation Measurements 37*, 377–381.

Murray, A. S., Marten, R., Johnson, A. & Martin, P. 1987: Analysis for naturally occurring radionuclides at environmental concentrations by gamma spectrometry. *Journal of Radioanalytical and Nuclear Chemistry Articles 115*, 263–288.

Muru, M., Rosentau, A., Kriiska, A., Lõugas, L., Kadakas, U., Vassiljev, J., Saarse, L., Aunap, R., Küttim, L., Puusepp, L. & Kihno, K. 2017: Sea level changes and Neolithic hunter-fisher-gatherers in the Centre of Tallinn, southern coast of the Gulf of Finland, Baltic Sea. *The Holocene 27*, 917–928.

Muru, M., Rosentau, A., Preusser, F., Plado, J., Sibul, I., Jõeleht, A., Bjursäter, S., Aunap, R. & Kriiska, A. 2018: Reconstructing Holocene shore displacement and Stone Age palaeogeography from a foredune sequence on Ruhnu Island, gulf of Riga, Baltic Sea. *Geomorphology 303*, 434–445.

Neal, A. 2004: Ground-penetrating radar and its use in sedimentology: principles, problems and progress. *Earth-Science Reviews 66*, 261–330.

Ning, W., Andersson, P., Ghosh, A., Khan, M. & Filipsson, H. 2017: Quantitative salinity reconstructions of the Baltic Sea during the mid-Holocene. *Boreas 46*, 100–110.

Nirgi, T., Rosentau, A., Habicht, H.-L., Hang, T., Jonuks, T., Jõeleht, A., Kihno, K., Kriiska, A., Mustasaar, M., Risberg, J., Suuroja, S., Talviste, P. & Tõnisson, H. 2020: Holocene relative shore-level changes and Stone Age palaeogeography of the Pärnu Bay area, eastern Baltic Sea. *The Holocene 30*, 37–52.

Nomals, P. 1930: Gitijas nogulumi pie Ģipkas [Sediments of gyttja at Ģipka]. *Acta Universitatis Latvinensis, Lauksaimniecības fakultātes serija I. 4*, 5–82.

Phantuwongraj, S., Choowong, M., Nanayama, F., Hisada, K. I., Charusiri, P., Chutakositkanon, V., Pailoplee, S. & Chabangbon, A. 2013: Coastal geomorphic conditions and styles of storm surge washover deposits from Southern Thailand. *Geomorphology 192*, 43–58.

Reimer, P. and 41 others 2020: The IntCal20 Northern Hemisphere radiocarbon age calibration curve (0–55 cal kBP). *Radiocarbon 62*, 725–757.

Risberg, J., Alm, G. & Goslar, T. 2005: Variable isostatic uplift patterns during the Holocene in southeast Sweden, based on high-resolution AMS radiocarbon datings of lake isolations. *The Holocene 15*, 847–857.

Roberts, H. M. & Wintle, A. G. 2001: Equivalent dose determinations for polymineralic fine-grains using the SAR protocol: application to a Holocene sequence of the Chinese Loess Plateau. *Quaternary Science Reviews 20*, 859–863.

Rosentau, A., Muru, M., Kriiska, A., Subetto, D. A., Vassiljev, J., Hang, T., Gerasimov, D., Nordqvist, K., Ludikova, A., Lougas, L., Raig, H., Kihno, K., Aunap, R. & Letyka, N. 2013: Stone age settlement and Holocene shore displacement in the Narva-Luga Klint Bay area, eastern Gulf of Finland. *Boreas 42*, 912–931.

Rosentau, A., Vassiljev, J., Hang, T. & Kalm, V. 2009: Development of the Baltic Ice Lake in the eastern Baltic. *Quaternary International 206*, 16–23.

Rosentau, A., Veski, S., Kriiska, A., Aunap, A., Vassiljev, J., Saarse, L., Hang, T., Heinsalu, A. & Oja, T. 2011: Palaeogeographic model for the SW Estonian coastal zone of the Baltic Sea. *In* Harff, J., Björck, S. & Hoth, P. (eds.): *The Baltic Sea Basin*, 165–188. Springer, Heidelberg, Dordrecht, Berlin, New York.

Saarse, L., Heinsalu, A. & Veski, S. 2009: Litorina Sea sediments of ancient Vääna Lagoon, northwestern Estonia. *Estonian Journal of Earth Sciences 58*, 85–93.

Saarse, L., Vassiljev, J. & Miidel, A. 2003: Simulation of the Baltic Sea shorelines in Estonia and neighbouring areas. *Journal of Coastal Research 19*, 261–268.

Saarse, L., Vassiljev, J., Rosentau, A. & Miidel, A. 2007: Reconstructed late glacial shore displacement in Estonia. *Baltica 20*, 35–45.

Sander, L., Fruergaard, M., Koch, J., Johannessen, P. N. & Pejrup, M. 2015: Sedimentary indications and absolute chronology of Holocene relative sea-level changes retrieved from coastal lagoon deposits on Samsø, Denmark. *Boreas 44*, 706–720.

Sandgren, P., Subetto, D., Berglund, B. E., Davydova, N. N. & Savelieva, L. A. 2004: Mid-Holocene Littorina Sea transgressions based on stratigraphic studies in coastal lakes of NW Russia. *GFF 126*, 363–380.

Seppä, H., Tikkanen, M. & Shemeikka, P. 2000: Late-Holocene shore displacement of the Finnish south coast: diatom, litho- and chemostratigraphic evidence from three isolation basins. *Boreas 29*, 219–231.

Smith, C., Soreghan, G. S. & Ohta, T. 2018: Scanning electron microscope (SEM) microtextural analysis as a paleoclimate tool for fluvial deposits: a modern test. *Bulletin of the Geological Society of America 130*, 1256–1272.

Snoeijs, P. 1993: *Intercalibration and Distribution of Diatom Species in the Baltic Sea 1*. 130 pp. Opulus Press, Uppsala.

Snoeijs, P. & Balashova, J. 1998: *Intercalibration and Distribution of Diatom Species in the Baltic Sea 5*. 126 pp. Opulus Press, Uppsala.

Snoeijs, P. & Kasperovičienė, J. 1996: *Intercalibration and Distribution of Diatom Species in the Baltic Sea 4*. 126 pp. Opulus Press, Uppsala.

Snoeijs, P. & Potapova, M. 1995: *Intercalibration and Distribution of Diatom Species in the Baltic Sea 3*. 126 pp. Opulus Press, Uppsala.

Snoeijs, P. & Vilbaste, S. 1994: *Intercalibration and Distribution of Diatom Species in the Baltic Sea 2*. 126 pp. Opulus Press, Uppsala.

Stabell, B. 1985: The development and succession of taxa within the diatom genus Fragilaria Lyngbye as a response to basin isolation from the sea. *Boreas 14*, 273–286.

Šturms, E. 1937: Neolīta apmetne Dundagas Purciemā [Neolithic settlement at Dundagas Pūrciems]. *Senatne un Māksla 1*, 46–54.

Tushingham, A. M. & Peltier, W. R. 1992: Validation of the ICE-3G Model of Würm-Wisconsin deglaciation using a Global Data Base of relative sea level histories. *Journal of Geophysical Research Atmospheres 97*, 3285–3304.

Veinbergs, I. 1996: Baltijas baseina attīstības vēsture leduslaikmeta beigu posmā un pēcleduslaikmetā pēc Latvijas piekrastes un tai pieguļošās akvatorijas pētījumu materiāliem [Developmental history of the Baltic Basin in the final stage of the glacial and the postglacial based on evidence from the Latvian coast and the adjacent seabed], *Report in Latvian State Geological Fond VĢF, Typing, nr 11544*, 82–84.

Velichkevich, F. U. & Zastawniak, E. 2006: *Atlas of the Pleistocene Vascular Plant Macrofossils of Central and Eastern Europe, Part 1: Pteridophytes and Monocotyledons*. 224 pp. W. Szafer Institute of Botany, Polish Academy of Sciences, Krakow.

Velichkevich, F. U. & Zastawniak, E. 2008: *Atlas of Pleistocene Vascular Plant Macrofossils of Central Europe*. Part 2: Herbaceous Dicotyledones. 380 pp. W. Szafer Institute of Botany, Polish Academy of Sciences, Krakow.

Vestøl, O., Ågren, J., Steffen, H., Kierulf, H. & Tarasov, L. 2019: NKG2016LU: a new land uplift model for Fennoscandia and the Baltic region. *Journal of Geodesy 93*, 1759–1779.

Vos, K., Vandenberghe, N. & Elsen, J. 2014: Surface textural analysis of quartz grains by scanning electron microscopy (SEM): from sample preparation to environmental interpretation. *Earth-Science Reviews 128*, 93–104.

Wang, Z., Zhan, Q., Long, H., Saito, Y., Gao, X., Wu, X., Li, L. & Zhao, Y. 2013: Early to mid-Holocene rapid sea-level rise and coastal response on the southern Yangtze delta plain, China. *Journal of Quaternary Science 28*, 659–672, https://doi.org/10.1002/jqs.2662.

Witkowski, A., Lange-Bertalot, H. & Metzeltin, D. 2000: Diatom flora of marine coasts I. *Iconographia Diatomologica 7*, 1–925.

Yu, S. Y., Berglund, B. E., Andrén, E. & Sandgren, P. 2004: Mid-Holocene Baltic Sea transgression along the coast of Blekinge, SE Sweden—ancient lagoons correlated with beach ridges. *GFF 126*, 257–272.

Yu, S., Berglund, B., Sandgren, P. & Lambeck, K. 2007: Evidence for a rapid sea-level rise 7600 yr ago. *Geology 35*, 891–894.

Supporting Information

Additional Supporting Information to this article is available at http://www.boreas.dk.

Fig. S1. Detrended Correspondence Analysis (DCA) ordination plot of the Ģipka section diatom percentage record, DCA axes 1 and 2. Samples are clustered based on diatom composition similarities. Samples close to each other suggest similar communities and are coloured according to salinity preference. Sample numbers are according to their modelled age (cal. a BP). Diatom assemblage zones presented in Fig. 3 are marked in the diagram by I–VIII.

Fig. S2. Micrographs of the selected grain outlines and microtextures on grain surfaces: A, subrounded grain; B, rounded grain; C, angular grain; D, conchoidal features on a grain (arrow); E, straight and arcuate steps; F, crescentic marks; G, V-shaped percussion marks (arrows); H, precipitation with holes and solution pits; I, oriented etch pits on different surfaces of crystallization (arrows); J, oriented etch pits on grain surface; K, medium relief grain; L, high relief grain.

Table S1. Diatom assemblage zones (DAZ) of the Ģipka sediment succession.

Table S2. Plant macrofossils from the Ģipka sediment succession.

Table S3. RSL data for the Ģipka and Ruhnu Island areas in the HOLSEA database format.

Table S4. List of radiocarbon dates and dated material from Pūrciems archaeological site (samples from 1930s excavation, held at the National History Museum of Latvia). For description of pottery wares, see Bērziņš (2008).